14 January 2014

ATRAP Progress

2012 Progress Report by the Antihydrogen TRAP Collaboration (ATRAP)

G. Gabrielse[1], **J. DiSciacca, S. Ettenauer, C. Hamley, N. Jones**
K. Marable, M. Marshall, E. Tardiff, R. Kalra
Department of Physics, Harvard University, Cambridge, MA 02138 USA

Walter Oelert, Dieter Grzonka, Thomas Sefzick, Marcin Zielinski
Institut für Kernphysik, Forschungszentrum Jülich, Germany

Eric Hessels, Cody Storry, Daniel Fitzakerley,
Matthew George, Matthew Weel
Department of Physics and Astronomy, York University,
Toronto, Ontario, M3J 1P3, Canada

A. Müllers[2], **J. Walz**[2]
Institute für Physik, Johannes Gutenberg Universität Mainz, D55099, Mainz, Germany

Marcin Zielinski
Institute of Physics, Jagiellonian University, Kraków, Poland

CERN-SPSC-2014-003 / SPSC-SR-130
13/01/2014

[1]spokesperson,gabrielse@physics.harvard.edu
[2]antihydrogen studies only

Contents

A. Introduction

Since no antiprotons were available in 2014 the SPSC has asked that the progress reports for this year focus upon giving a summary of the ATRAP program, with a particular emphasis on the major apparatus in place and planned, and relating these to the measurement goals for the collaboration.

B. Review of Motivations

1. Tests of CPT Invariance

Whether reality is invariant under CPT transformations is fundamentally an experimental question. A primary motivation for this research program is to use precise laser spectroscopy to probe for tiny difference between antihydrogen ($\overline{\mathrm{H}}$) and hydrogen atoms, thereby providing the most sensitive tests of CPT invariance with baryons and leptons.

Experimental tests have made physicists abandon widely held but mistaken assumptions about fundamental symmetries – first that reality is invariant under P transformations and second that reality is invariant under CP transformations. The current assumption, that reality is invariant under CPT, is based in large part upon the success of quantum field theories (QFT) for which there is a CPT theorem if plausible assumptions (like causality, locality and Lorentz invariance) are made. Of course, this argument cannot be universal since gravity does not fit into a QFT.

String theory has no intrinsic CPT invariance except when taken to the limit of a quantum field theory. Theoretical investigations of possible CPT violations have thus been studied in the context of string theory [1, 2]. One widely used parametrization [3] considers standard model extensions that arise if Lorentz violations are not excluded, whether these originate in string theory or elsewhere. Quantitative comparisons of existing CPT tests and possible $\overline{\mathrm{H}}$ measurements [4] were provided.

A reasonable requirement for a CPT test with $\overline{\mathrm{H}}$ and H is that it eventually be more stringent than existing tests with leptons and baryons. Table 1 distinguishes the precision of the CPT test from the measurement precision since these can be very different. The most precise baryon CPT test is the 9×10^{-11} (90 ppt) comparison of the charge-to-mass ratios of the $\overline{\mathrm{p}}$ and p carried out as part of this research program [5]. For that measurement, as for proposed $\overline{\mathrm{H}}$ and H comparisons, the CPT test accuracy is the same as the measurement accuracy, so extremely precise measurements are required to probe CPT invariance at an interesting precision.

Table 1: Comparing the Precise CPT Tests for the Three Species of Particles

	CPT Test Accuracy	Measurement Accuracy	Enhancement Factor
Mesons ($K_0\bar{K}_0$)	2×10^{-18}	2×10^{-3}	10^{15}
Leptons (e^+e^-)	2×10^{-12}	2×10^{-9}	10^3
Baryons ($p\bar{p}$)	9×10^{-11}	9×10^{-11}	1

The most accurate direct tests of CPT invariance are represented in Table 1 and Figs. 1-2. The CPT tests with leptons and mesons involve free enhancement factors that make the precision of the CPT test substantially greater than the measurement precision. The most precise lepton CPT test is a 2×10^{-9} comparison of measured magnetic moment anomalies of electron and positron [6], interpreted as a comparison of magnetic moments at 2×10^{-12}. A single meson CPT test is even more precise [7]. The delicately balanced nature of the unique kaon system makes it possible to interpret a measurement precision of only 2×10^{-3} as a comparison of the masses of the K_0 and $\bar{K}_0$

to an astounding 2×10^{-18}. One theoretical suggestion [1] is that quantum gravity could produce a CPT violation which is smaller by about a factor of 10.

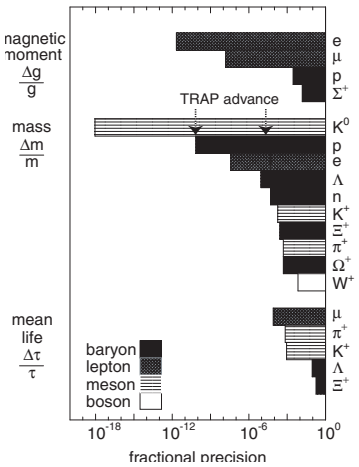

Figure 1: CPT Tests (primarily from the Particle Data Group compilation). Charge-to-mass ratio comparisons are included in "mass" measurements.

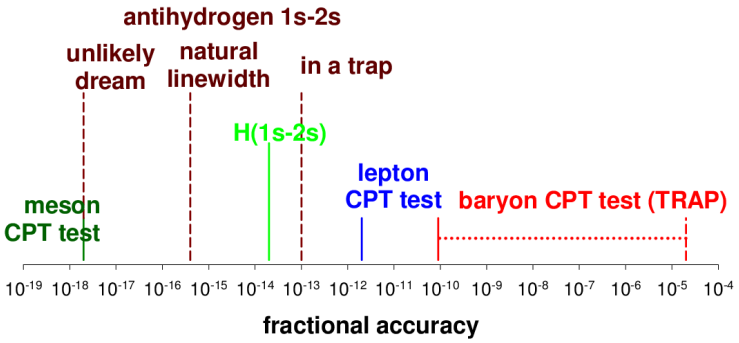

Figure 2: Relevant accuracies for the precise 1s - 2s spectroscopy of antihydrogen are compared to the most stringent tests of CPT invariance carried out with the three types of particles: mesons, leptons and baryons.

2. Antihydrogen Spectroscopy Offers the Prospect of Higher Accuracy CPT Test with Leptons and Baryons

In principle, the comparisons of $\overline{\mathrm{H}}$ and H could make possible a CPT test at the meson precision. The 1s-2s transition has an extremely narrow fractional linewidth of only 5×10^{-16}. With a measurement signal-to-noise ratio of 200, line splitting by this factor would allow a comparison at the kaon precision. There are serious obstacles to attaining this extremely high precision, however, including a small number of available anti-atoms, a 2.4 mK laser cooling limit, a second-order Doppler shift, and possible Zeeman shifts depending on the configuration of the magnetic trap. Nonetheless, even a measurement at an accuracy of 10^{-13}, the level at which the difficulties mentioned may be manageable in the first traps [8], would give a substantially improved CPT test involving leptons and baryons.

The most precise laser spectroscopy of hydrogen attained so far [9] was obtained with a hydrogen beam by one group in this collaboration [10]. The narrowest observed width is still much wider than the natural linewidth (Fig. 2) but we expect that steady and substantial improvements in accuracy will continue as they have been for many years. If such a narrow line were available for $\overline{\mathrm{H}}$ as well as H, the signal-to-noise ratio would be sufficient to allow the frequencies to be compared to at least 1 part in 10^{13}, a large increase in precision over the current tests involving baryons and leptons. The first use of cold trapped H for 1s-2s spectroscopy [11], in an environment similar in many respects to that we hope to arrange for $\overline{\mathrm{H}}$, comes very close to this linewidth, with substantial improvements expected if laser jitter had been reduced.

The ratio of the 1s-2s transition frequencies determine a ratio of Rydberg constants. In terms of other fundamental constants,

$$\frac{R_\infty(\bar{H})}{R_\infty(H)} = \frac{m[e^+]}{m[e^-]} \left(\frac{q[e^+]}{q[e^-]}\right)^2 \left(\frac{q[\bar{p}]}{q[p]}\right)^2 \frac{1 + m[e^+]/M[\bar{p}]}{1 + m[e^-]/M[p]}$$

(assuming the long range Coulomb interaction is the same for $\bar{H}$ and H). The only ratios on the right that have been measured accurately are the electron-to-proton mass ratio and the ratio of the electron and proton charges. This CPT test comparison thus clearly involves fundamental lepton and baryon constants but in a combination which makes it difficult to simply interpret the comparison as a measurement of the electron-to-positron mass ratio, or any other such simple ratio. The comparison of 1s-2s transition frequencies measured for $\overline{\mathrm{H}}$ and H would be a test of CPT invariance that involves the charges and masses of leptons and baryons at an unprecedented precision. Fig. 2 shows how the precision scales for $\overline{\mathrm{H}}$ 1s - 2s spectroscopy (mentioned above) compares favorably with that attained in existing CPT tests with leptons, mesons and baryons.

3. Gravitational Force on Antimatter

A second motivation for experiments which compare cold $\overline{\mathrm{H}}$ and H is the possibility to search for differences in the force of gravity upon antimatter and matter [12]. Making gravitational measurements with neutral $\overline{\mathrm{H}}$ certainly seems much more feasible than using charged $\overline{\mathrm{p}}$, for which the much stronger Coulomb force masks the weak gravitational force. Depending upon how cold is the antihydrogen we eventually achieve, it may be possible to measure the gravitational force on trapped $\overline{\mathrm{H}}$ [13], by adapting methods for measuring the free fall of cold atoms released from a trap [14], perhaps by ionizing H^- with a laser just above threshold, after first sympathetically cooling them to an extremely low temperature in an ion trap [15]. We are intrigued by the possibility of experimental comparisons of the force of gravity upon $\overline{\mathrm{H}}$ and H, and will pursue this direction when the techniques are sufficiently advanced to permit attaining an interesting level of precision.

However, it seems very unlikely that one can attain the precision that we at TRAP attained [16] in comparing the gravitational red shift of an antiproton cyclotron clock with a proton clock [17]. This comparison showed that gravity is the same for a proton and antiproton to 1 part in 10^6.

C. ATRAP History, Goals and Status

1. ATRAP History and Methods

Especially for the sake of new members to the SPSC, we note that the basic antiproton methods now used by all antihydrogen and antiproton collaborations were developed by the TRAP collaboration which evolved into ATRAP. Antiprotons were slowed in matter and trapped with the sudden application of a potential [18]. The antiprotons were then cooled with electrons to produce antiproton energies about 10^{10} times lower than had previously been produced. Antiproton accumulation (called stacking) was demonstrated soon after [19] and later reported in detail [20]. CERN's Antiproton Decelerator(AD) was built so that the antihydrogen aspirations could be realized. Five collaborations approved by the SPSC are using or planning to use these methods.

The proposal to make cold antihydrogen using cold, trapped antiprotons was laid out by some of us in the TRAP collaboration back in 1987 [21], not long after the first antiprotons were trapped [18]. The production of antihydrogen cold enough to capture in a neutral particle trap for precise laser spectroscopy was proposed at the same time.

2. The Dual ATRAP Goals Remain the Same

From its beginning, ATRAP announced, pursued, and reported to the SPSC each year on two long term goals. These goals were laid out by some of us long ago. They have not changed.

1. Producing cold antihydrogen, trapping cold antihydrogen in its ground state, laser cooling the trapped antihydrogen, and performing precise spectroscopic and gravitational comparisons of trapped antihydrogen and hydrogen.

2. Making precise comparisons of the properties of the antiproton and the proton – their magnetic moments and their charge-to-mass ratios in particular.

In subsequent sections we discuss the ATRAP antiproton beam line that was built with two ports to make it possible to purse both goals simultaneously. Almost all of the available antiprotons go to the antihydrogen experiments. However, a small fraction of the antiprotons can be skimmed off as often as once per day, or as seldom as once per month, as needed.

3. Status of Precise Comparisons of the Antiproton and the Proton

Magnetic Moments

Preparations for the ATRAP antiproton magnetic moment measurement were carried out at Harvard. In 2010, the first observations of self-excitation and feedback cooling of a single trapped proton were reported [22]. In 2012 the first one-particle measurement of the proton magnetic moment was reported [23].

In 2013, ATRAP made the first one-particle measurement of the antiproton magnetic moment, the only such measurement so far, achieving a 680 times more precise measurement than had been realized with any other method. Our report on this measurement [24] was widely celebrated.

Great additional improvements in precision, perhaps as much as 1000 to 10,000, may be possible with the use of quantum methods. A demonstration experiment that made use of one trapped antiproton demonstrated that individual spin flips of a single antiproton could be observed [25].

The antiproton magnetic moment apparatus used to make the first one-particle comparison of the antiproton and proton is currently available for proton operation at CERN, and for antiprotons once they again become available. In addition, work is progressing at Harvard on improved apparatus and methods.

Charge-to-Mass Ratios

A series of three comparisons of the charge-to-mass ratios of the antiproton and proton were carried out at LEAR [19, 5, 16]. The measurements were made by the TRAP collaboration, that later expanded to become ATRAP. To complete these measurements, TRAP developed methods to slow, capture and cool antiprotons. These are the antiproton methods that have since made all of the AD antihydrogen experiments possible.

The most precise comparison of the charge-to-mass ratios of the antiproton and proton showed that these have the opposite sign with the same magnitude to 9 parts in 10^{11}. This is by far the most sensitive test of CPT invariance for a baryon system. Most of this final measurement was done with one antiproton just two weeks before LEAR closed. It is likely that the q/m comparison could now be done more precisely.

ATRAP plans to do such measurements in the same traps used for antiproton magnetic moment measurements, when time permits. However, the magnetic moment measurements have the highest priority given that they have so far been measured much less precisely than the charge-to-mass ratios.

4. Status of the Antihydrogen Program

ATRAP has reported the observation of 5 trapped, ground state antihydrogen atoms per trial [26]. A 2013 report discusses how electric fields were used to avoid mirror-trapped antiprotons [27]. The 5 atoms per trial is substantially more antihydrogen per trial than has otherwise been realized, but more trapped atoms per trial are needed. We believe that we have developed the methods to make this possible once our second generation Ioffe trap is operational.

The next objective (once antiprotons are again available) is to demonstrate three dimensional laser cooling of trapped antihydrogen atoms. Doing this most effectively requires a Penning-Ioffe

trap which has sideports (perpendicular to the magnetic field direction) to admit coherent Lyman alpha radiation at 121 nm into the trap.

Our first generation Ioffe trap was the first to have such openings into a antihydrogen trap, but the technology of this trap prevented it from being used for more than a trial or two during an 8 hour beam shift. Our second generation trap has the capacity to be used repeatedly during a beam shift as well having sideports.

The difficulties we had the vacuum system for the second generation Ioffe trap were carefully documented with the SPSC. The defective vacuum enclosure has now been removed without damaging the trap windings. Extensive electrical tests of the second generation Ioffe trap, stripped from the faulty vacuum system, demonstrate that it performs at essentially its designed electrical specifications. We are on schedule to have it enclosed in a new metal vacuum system and ready for the 2014 beam run.

Such setbacks are very unpleasant but are the occasional cost of operating close to the technology frontier of what is possible. For the 25 years that some of us have been working at CERN we have often been using new apparatus and methods that push technology hard. Despite our recent setback, most of our efforts have succeeded, with the result that the AD antihydrogen program relies on the methods that we earlier invented and demonstrated.

The ATRAP trap apparatus other than new Ioffe trap vacuum enclosure will not differ significantly from what was used earlier and described to the SPSC. High current power supplies, located on the zone 2 platform, are in place and fully tested, for supplying hundreds of amps to the second generation trap.

D. ATRAP Apparatus: Overview, Status and Immediate Plans

To allow the simultaneous pursuit of ATRAP's dual goals, as discussed above, the ATRAP beamline was built with two ports. The precision antiproton measurement require antiprotons

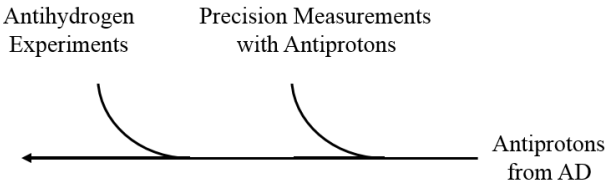

Figure 3: The ATRAP beamline has two antiproton ports – one for antihydrogen experiments (delineated with the red circle) and the second for antiproton experiments (delineated with the blue circle).

much less frequently since we have demonstrated that antiprotons can be stored for such measurement for weeks and even months at a time without reloading. Most of the antiprotons thus are used for antihydrogen experiments.

The ATRAP experimental area is divided into three experimental zones which are radiation controlled. A top view of these areas is represented in Fig. 5. Antiprotons are available for precise antiproton experiments in zone 1. The most sensitive control and detection electronics for this zone are in an adjacent Faraday cage – both within the red dotted lines in the figure. Antiprotons are available for antihydrogen experiments in zone 2. The most sensitive control and detection electronics for this zone are also in an adjacent Faraday cage – both within the blue dotted lines in the figure. The positrons needed to make antihydrogen are produced in zone 3, within the green dotted lines in the figure. The lasers needed for antihydrogen production are located in a third Faraday cage, labeled as "laser cabin" within the dotted yellow lines in the figure.

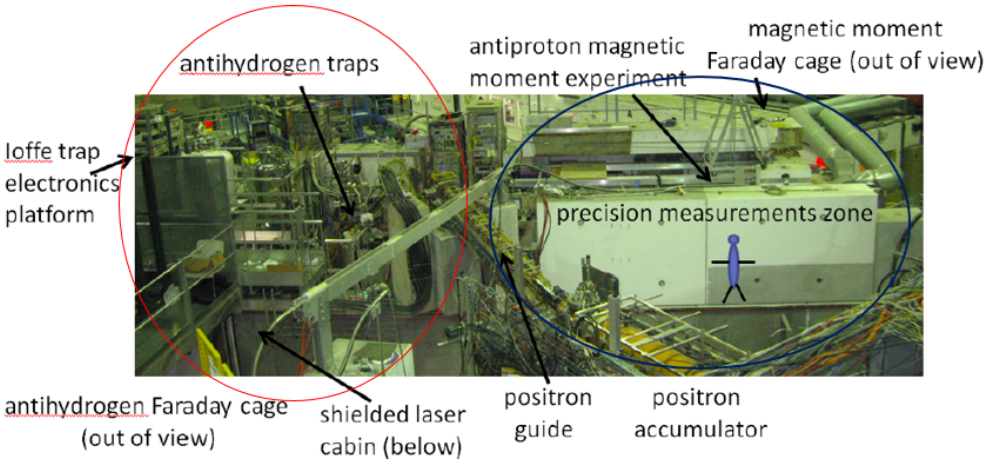

Figure 4: Photograph of the ATRAP beamline with two antiproton ports – one for antihydrogen experiments and the second for antiproton experiments.

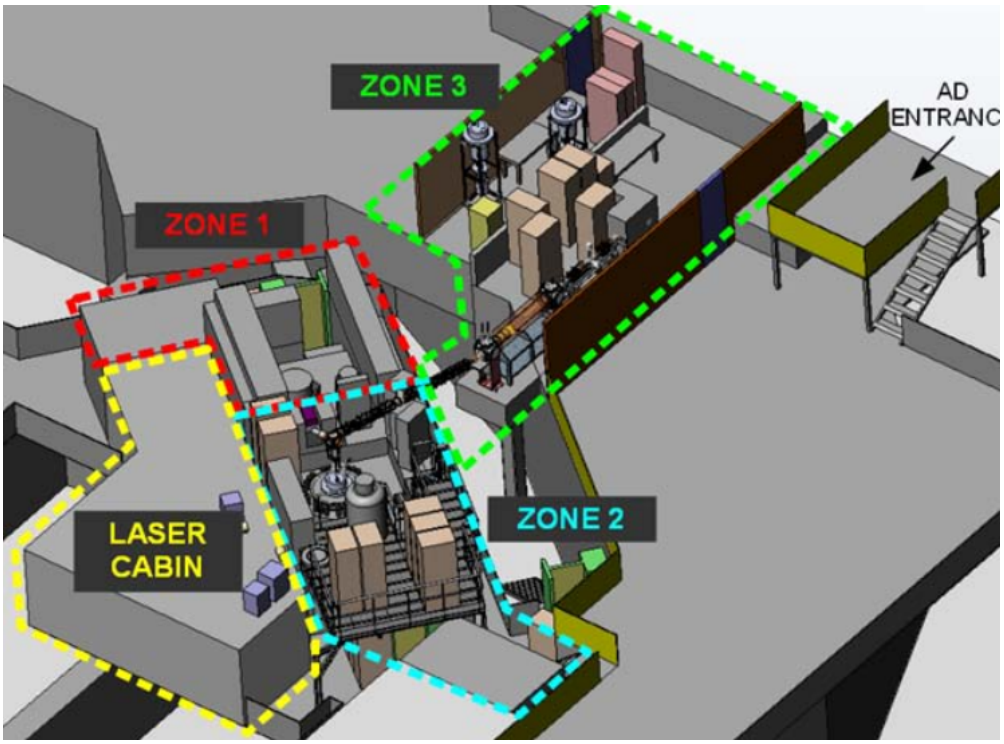

Figure 5: Top representation of the three ATRAP experimental areas. Antiprotons are available for precise antiproton experiments (zone 1) and for antihydrogen experiments (zone 2). The positrons needed to make antihydrogen are produced in third area (zone 3).

In response to the SPSC request for this report, we next present more detailed drawings that we hope will allow the committee members to better understand the ATRAP experimental layout.

1. Zone 1: For Precise Comparisons of Antiprotons and Protons

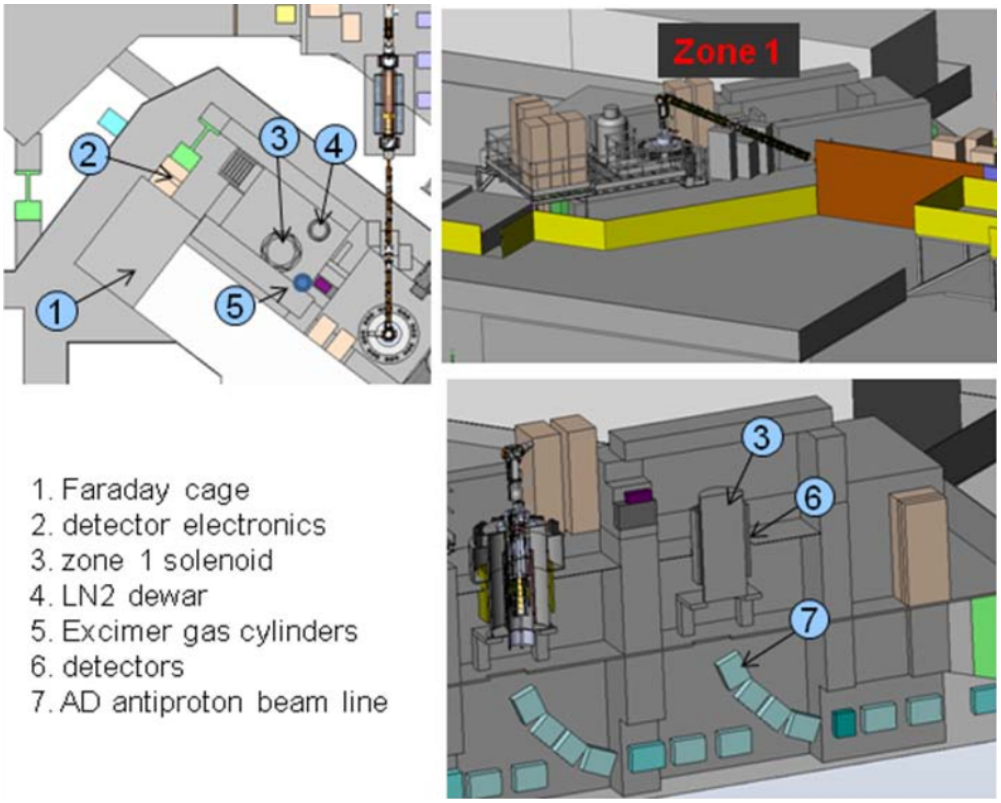

Figure 6: Precise comparisons of antiprotons and protons take place in ATRAP zone 1.

2. Zone 2: Antihydrogen

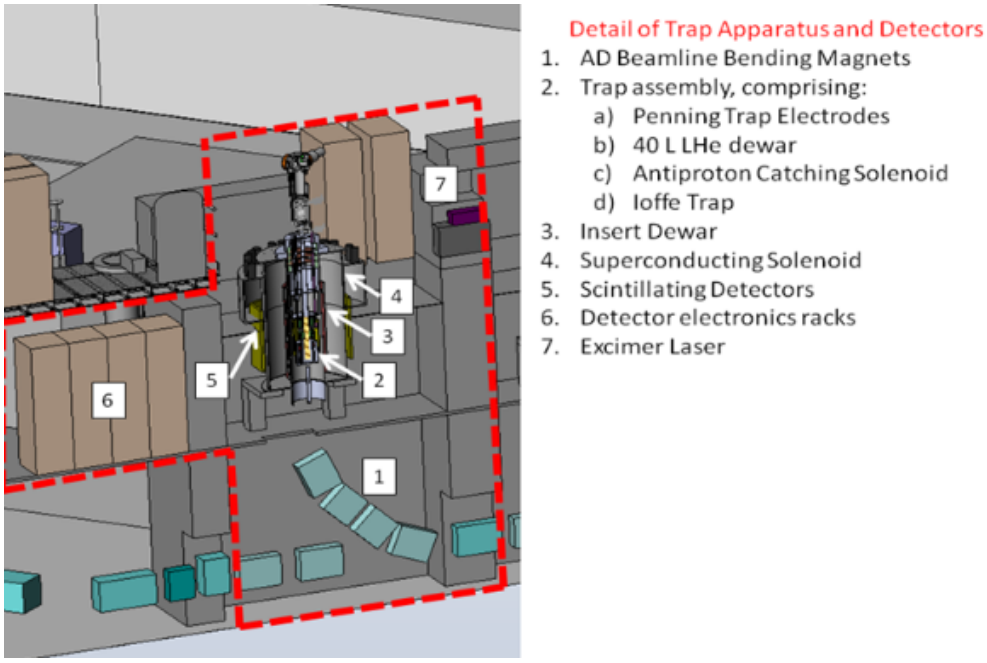

Figure 7: Antidhyrogen production and studies take place in ATRAP zone 2.

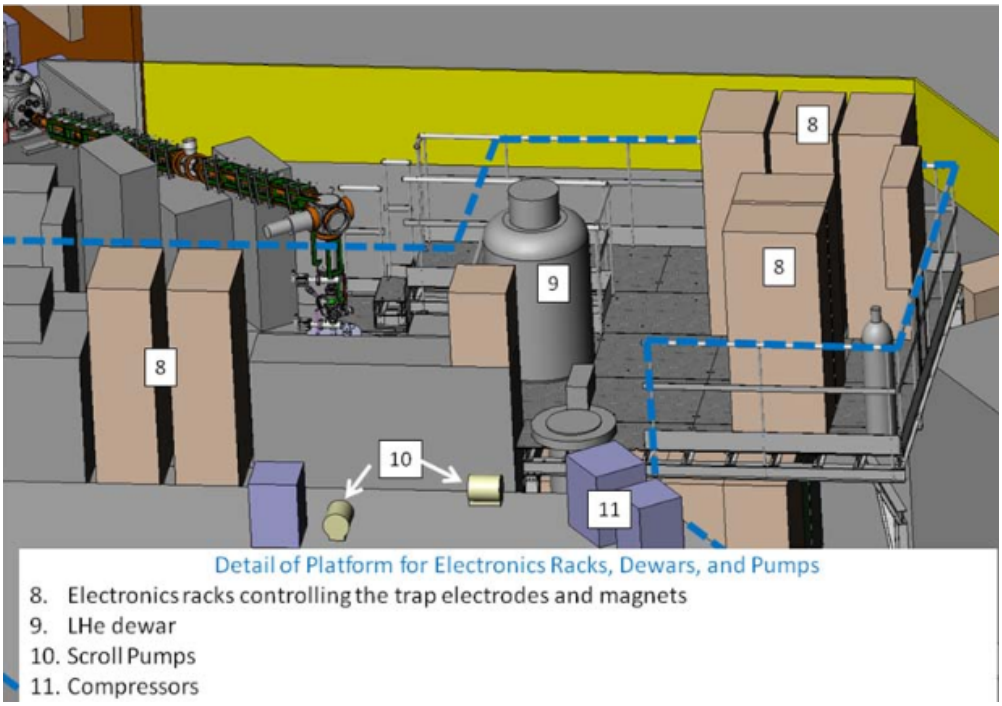

Figure 8: The antihydrogen production area (ATRAP zone 2) includes a platform on which supporting electronics and cryogen dewars are stored.

3. Zone 3: Positron Production for Antihydrogen

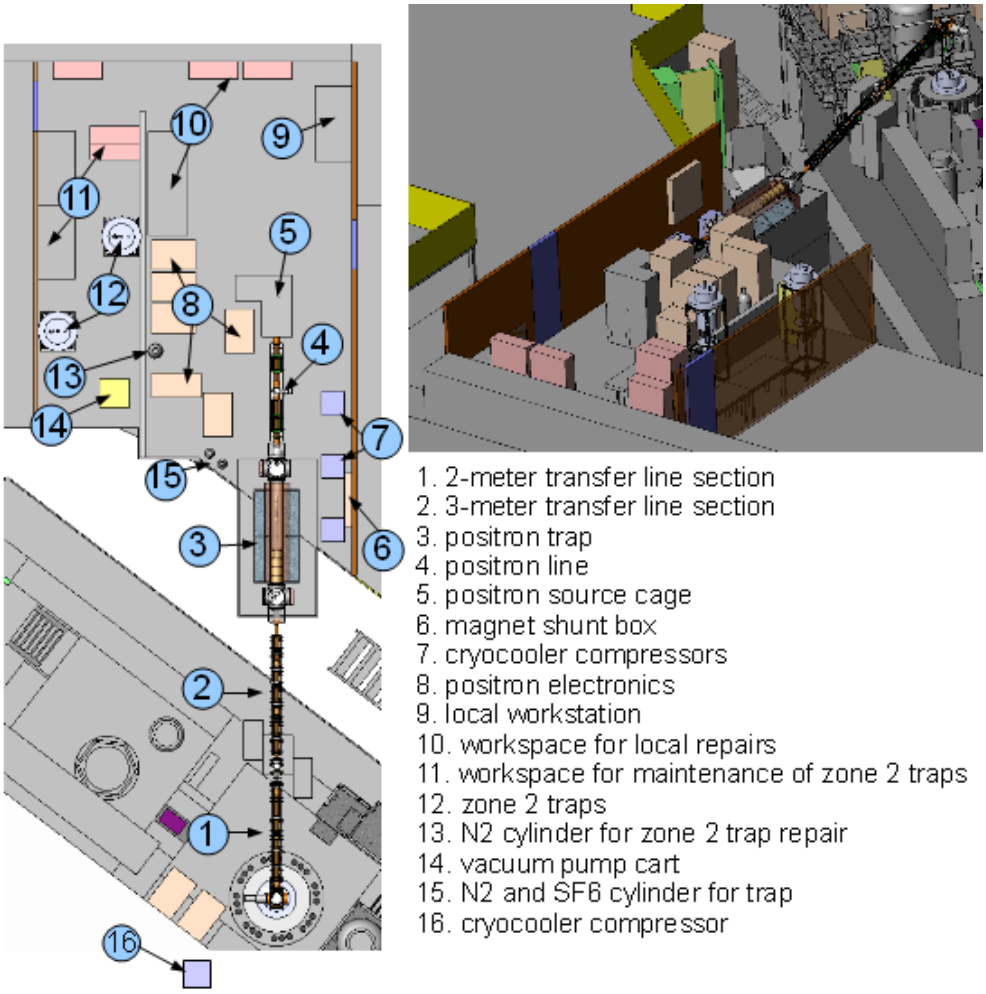

Figure 9: Positron production for antihydrogen production takes place in ATRAP zone 3.

4. Laser Faraday Cage

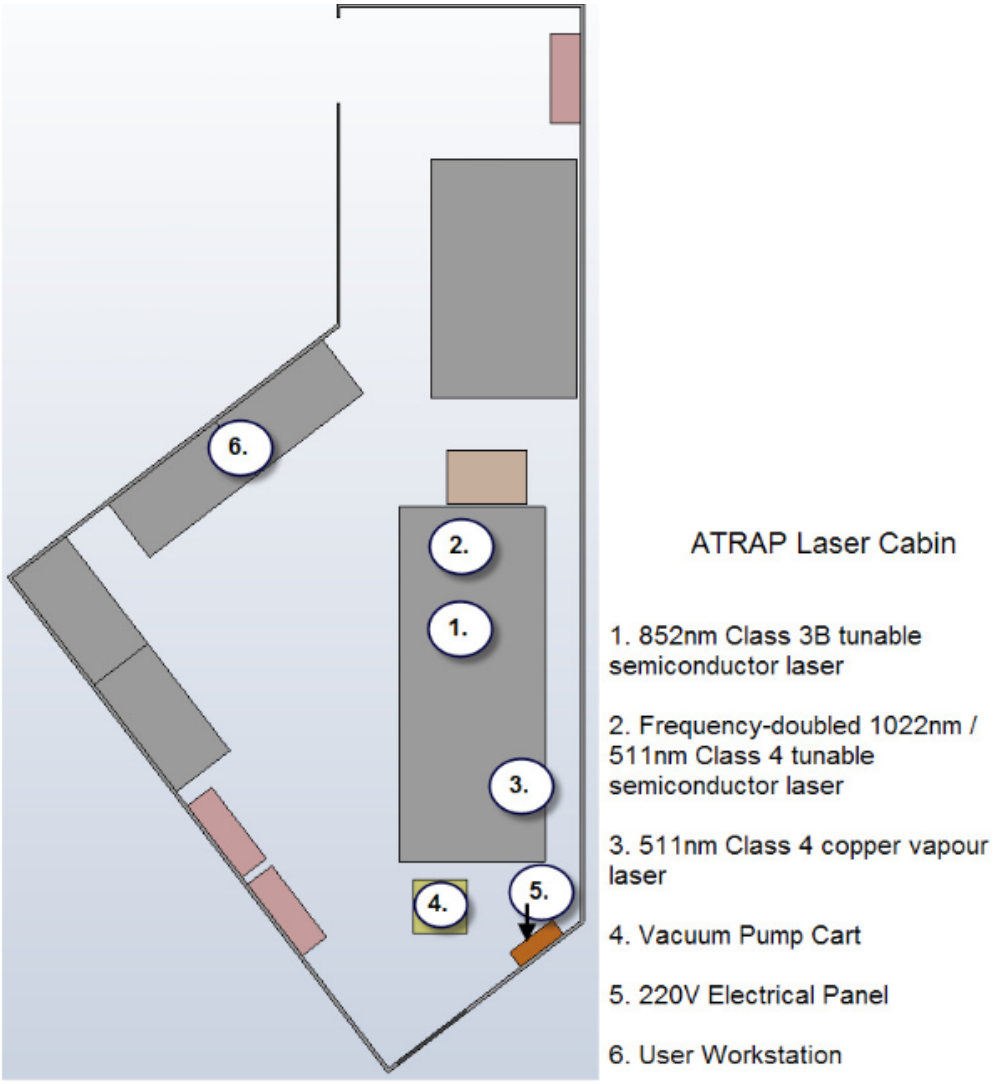

Figure 10: A third Faraday cage contains two laser tables. Lasers on these tables have so far been used for laser-controlled charge exchange production of antihydrogen. Two additional laser systems will be brought to CERN and installed in this laser cabin when these are needed.

Two additional laser systems are critical for the future objectives of ATRAP. Both of these systems are operating in the laboratories of collaboration members.

1. A continuous, coherent 121 nm Lyman alpha system is operating at the University of Mainz. It is intended for 3-dimensional cooling of trapped antihydrogen atoms, and for initial spectroscopy.

2. A continous 243 nm laser system is operating at Harvard. It will be used for for 1s-2s spectroscopy of trapped antihydrogen.

The current plan is to continue development of the laser systems at member institutions until they are transfered to the laser cabin for use at CERN. Discussion of the optimal time for moving these systems are taking place within the collaboration.

E. Manpower

The ATRAP collaboration at the AD, and the TRAP collaboration at LEAR from which it developed, have both always been small compared to the collaborations with which they have competed at LEAR and the AD.

Over the years we have demonstrated that a small team can compete effectively. Our small teams developed and demonstrated the cold antiproton methods upon which the current AD collaborations rely, as has been mentioned. The only precise comparisons of antimatter and matter systems have been carried out by the small TRAP and ATRAP teams:

1. Comparison of the charge-to-mass ratios of the antiproton and proton to 9 parts in 10^{11}
2. Comparison of antiprotons and proton gravity to 1 part in 10^6 using the gravitational red shift
3. Comparison of the antiproton and proton magnetic moment to 5 parts in 10^6.

(No comparisons of antihydrogen and hydrogen have yet been carried out.)

While effective for precision measurements, the small size of our collaboration does reduce the rate at which we can build new apparatus, and does make it difficult to build and/or develop apparatus during antiproton beam time. With a larger team, for example, we likely would have been able to recover more quickly from the failure of the Ioffe trap vacuum enclosure.

A new group has joined our collaboration to take over some of the detector maintenance for which our Juelich collaborators have been responsible. In addition we are beginning discussions with a view to expanding the ATRAP collaboration. Partly this is required just for us to keep up. The antihydrogen collaborations that we compete with, and the new collaboration organized to compete with us on precise antiproton/proton comparisons, are both much larger than we are. There are also several areas where we could use some help and expertise, especially as the ELENA time approaches.

F. Not the Usual CERN Experiment

Especially for the sake of new SPSC members, it is important to note that the low-energy, high precision antihydrogen research differs substantially from the normal high energy particle and nuclear physics experiments that are practiced so successfully at CERN. Most CERN experiments are carefully crafted so that with a large number of particles delivered to an interaction region over some years, a signal of a particular interaction or particle will be established (or not) at a desired and predictable level of statistical accuracy.

Antihydrogen experiments, like most highly accurate low-energy experiments, are very different. Most of the experimental time is spent in inventing new techniques and methods that make it possible to see a signal at all. A long sequence of short experiments require very precise control and preparation, but the result of one short experiment helps decide what short experiments will follow it. Longer term time schedules are thus less predictable than is normal for CERN high energy experiments. Once a signal is found, the accuracy attained is rarely statistical, being generally limited by systematic uncertainties.

Many other examples can be given for extremely precise measurements being realized after considerable time and effort. One is that the extremely accurate hydrogen spectroscopy experiments by an ATRAP collaborator who was recognized with the 2005 Nobel prize [28]. The recent electron magnetic moment measurement and the fine structure constant measurement made recently by another in our collaboration is another example [29].

In the past, some on the SPSC committee have had difficulty understanding the difference between the high energy experiments that they are involved in at CERN, and this low energy

antihydrogen research program. They have wanted time lines which show clearly and precisely what accuracy antihydrogen spectroscopy will be attained with what number of antiprotons delivered from the AD. It is important to realize that we spend most of our time at ATRAP inventing and refining new methods which eventually should make it possible to see and use an antihydrogen spectroscopy signal.

In some ways the situation is similar to the situation which pertained when the original TRAP Collaboration (PS196) proposed to accumulate antiprotons at an energy 10^{10} times lower than the lowest storage energy in the Low Energy Antiproton Ring, and to listen to the radio signal of a single antiproton as a way of the comparing antiproton and proton 45,000 time more accurately than had been done before. Despite the experience and expertise of the original collaboration, techniques demonstrated with matter particles had to be adapted for the very different circumstances under which antimatter particles were available. Most of the TRAP time and effort went into developing, demonstrating and improving apparatus and techniques, rather than into accumulating statistics with a fixed apparatus. There was some risk insofar as much had yet to be invented, but after a decade of concentrated effort by a small team, the ambitious goal was met and even substantially exceeded.

G. Three Recent ATRAP Papers

PRL 110, 130801 (2013) | Selected for a Viewpoint in *Physics* | PHYSICAL REVIEW LETTERS | week ending 29 MARCH 2013

One-Particle Measurement of the Antiproton Magnetic Moment

J. DiSciacca,[1] M. Marshall,[1] K. Marable,[1] G. Gabrielse,[1,*] S. Ettenauer,[1] E. Tardiff,[1] R. Kalra,[1] D. W. Fitzakerley,[2] M. C. George,[2] E. A. Hessels,[2] C. H. Storry,[2] M. Weel,[2] D. Grzonka,[3] W. Oelert,[3,4] and T. Sefzick[3]

(ATRAP Collaboration)

[1]*Department of Physics, Harvard University, Cambridge, Massachusetts 02138, USA*
[2]*Department of Physics and Astronomy, York University, Toronto, Ontario M3J 1P3, Canada*
[3]*IKP, Forschungszentrum Jülich GmbH, 52425 Jülich, Germany*
[4]*Institut für Physik, Johannes Gutenberg Universität Mainz, D-5509 Mainz, Germany*
(Received 21 January 2013; published 25 March 2013)

For the first time a single trapped antiproton ($\bar{p}$) is used to measure the $\bar{p}$ magnetic moment $\boldsymbol{\mu}_{\bar{p}}$. The moment $\boldsymbol{\mu}_{\bar{p}} = \mu_{\bar{p}}\boldsymbol{S}/(\hbar/2)$ is given in terms of its spin $\boldsymbol{S}$ and the nuclear magneton (μ_N) by $\mu_{\bar{p}}/\mu_N = -2.792\,845 \pm 0.000\,012$. The 4.4 parts per million (ppm) uncertainty is 680 times smaller than previously realized. Comparing to the proton moment measured using the same method and trap electrodes gives $\mu_{\bar{p}}/\mu_p = -1.000\,000 \pm 0.000\,005$ to 5 ppm, for a proton moment $\boldsymbol{\mu}_p = \mu_p\boldsymbol{S}/(\hbar/2)$, consistent with the prediction of the *CPT* theorem.

DOI: 10.1103/PhysRevLett.110.130801 PACS numbers: 14.20.Dh, 11.30.Er, 13.40.Em, 37.10.Ty

Measurements of the properties of particles and antiparticles are intriguing in part because the fundamental cause of the asymmetry between matter and antimatter in the universe has yet to be discovered. Within the standard model of particle physics, the results of particle-antiparticle comparisons are predicted by a *CPT* theorem [1] that pertains because systems are described by a local, Lorentz-invariant, quantum field theory (QFT). Whether the theorem applies universally is open to question, especially since gravitational interactions have so far eluded a QFT description. It is thus important to precisely test predictions of the *CPT* theorem, one example of which is that antiproton ($\bar{p}$) and proton (p) magnetic moments have opposite signs and the same magnitude. Testing this prediction may eventually produce a second precise *CPT* test with a baryon and antibaryon, of comparable precision to the $\bar{p}$ and p charge-to-mass ratio comparison [2].

The $\bar{p}$ magnetic moment was previously deduced only from measured transition energies in exotic atoms in which a $\bar{p}$ orbits a nucleus as a "heavy electron." Measurements 25 and 4 years ago [3,4] both reached a 3000 ppm precision (Fig. 1). Meanwhile, single particle methods were used to measure other magnetic moments to a much higher precision. For example, the most precisely measured property of an elementary particle is the electron magnetic moment measured with one electron [5].

This Letter reports the first single-particle measurement of the $\bar{p}$ magnetic moment, a 4.4 ppm determination that is 680 times more precise than realized with exotic atoms (Fig. 1). The methods and apparatus were initially demonstrated in a one-proton measurement of μ_p [6], following the realization of feedback cooling and a self-excited oscillator with one proton [7]. We profited from a parallel exploration of proton spin flips [8] and a measurement of μ_p [9] that followed ours.

The cyclotron and spin frequencies (f_c and f_s), measured for a single $\bar{p}$ suspended in a magnetic field, determine the $\bar{p}$ moment in nuclear magnetons,

$$\frac{\mu_{\bar{p}}}{\mu_N} \equiv \frac{g_{\bar{p}}}{2}\frac{q_{\bar{p}}/m_{\bar{p}}}{q_p/m_p} \approx -\frac{g_{\bar{p}}}{2} = -\frac{f_s}{f_c}, \tag{1}$$

where $g_{\bar{p}}$ is the $\bar{p}$ g factor. The ratio of $\bar{p}$ and p charge-to-mass ratios enters because the nuclear magneton μ_N is defined in terms of the proton charge and mass. This ratio was measured to be -1 to 0.0001 ppm using a $\bar{p}$

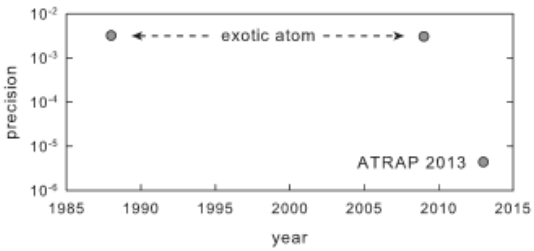

FIG. 1. Uncertainties in measurements of the $\bar{p}$ magnetic moment measured in nuclear magnetons, $\mu_{\bar{p}}/\mu_N$.

simultaneously trapped with a H^- ion [2] so the approximation in Eq. (1) is more than adequate for our precision.

The $\bar{p}$ magnetic moment is measured within the "analysis trap" electrodes (Fig. 2) used to measure the proton magnetic moment [6]. The stacked rings are made of OFE copper or iron, with a 3 mm inner diameter and an evaporated gold layer. The electrodes and surrounding vacuum container are cooled to 4.2 K by a thermal connection to liquid helium. Cryopumping of the closed system made the vacuum better than 5×10^{-17} Torr in a similar system [10], so collisions are unimportant. Appropriate potentials applied to electrodes with a carefully chosen relative geometry [11] make a very good electrostatic quadrupole near the trap center with open access to the trap interior from either end.

After the proton measurement [6] was completed, the apparatus was modified and moved from Harvard to CERN. The neighboring electrodes and vacuum enclosure (not pictured in Fig. 2) were modified to allow 5 MeV $\bar{p}$ from CERN's antiproton decelerator (AD) to enter the vacuum enclosure through a thin Ti window and to be captured and electron cooled in the neighboring electrodes. The cooling electrons are ejected by reducing the trap potential long enough that light electrons escape while heavier $\bar{p}$ do not. These methods, now used for all low energy $\bar{p}$ and $\bar{\mathrm{H}}$ experiments, are reviewed in Ref. [12].

Once the $\bar{p}$ is centered in the analysis trap, in a 5 tesla vertical magnetic field $\mathbf{B} = B\hat{\mathbf{z}}$, the circular cyclotron motion of a trapped $\bar{p}$ is perpendicular to $\mathbf{B}$ with a frequency $f_+ = 79.152$ MHz slightly shifted from f_c by the electrostatic potential. The $\bar{p}$ also oscillates parallel to $\mathbf{B}$ at about $f_z = 920$ kHz. The third motion is a circular magnetron motion, also perpendicular to $\mathbf{B}$, at the much lower

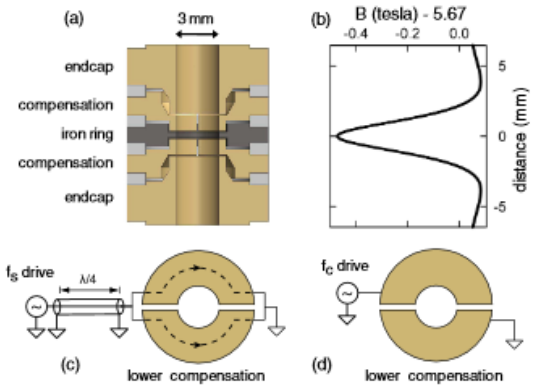

FIG. 2 (color online). (a) Electrodes of the analysis trap (cutaway side view) are copper with an iron ring. (b) The iron ring significantly alters B on axis. (c) Top view of the paths of the oscillating current for the spin flip drive. (d) An oscillating electric field (top view) drives $\bar{p}$ cyclotron motion.

frequency $f_- = 5.32$ kHz. The spin precession frequency is $f_s = 221.075$ MHz.

Driving spin flips requires a magnetic field perpendicular to $\mathbf{B}$ that oscillates at approximately f_s. This field is generated by currents (increased compared to Ref. [6] by a transmission line transformer) sent through halves of a compensation electrode [Fig. 2(c)]. Driving cyclotron transitions requires an electric field perpendicular to $\mathbf{B}$ that oscillates at approximately f_+. This field is generated by potentials applied across halves of a compensation electrode [Fig. 2(d)].

Much of the challenge of the measurement arises from the small size of a nuclear magnetic moment. Unlike the electron moment, which scales naturally as a Bohr magneton (μ_B), the nuclear moments scale as the much smaller nuclear magneton μ_N, with $\mu_N/\mu_B = m_e/m_p \sim 1/2000$. Shifts in f_z reveal changes in the cyclotron, spin, and magnetron quantum numbers n, m_s, and ℓ [13],

$$\frac{\Delta f_z}{f_z} = \frac{\hbar\beta_2}{4\pi m_p |B| f_-}\left(n + \frac{1}{2} + \frac{g_p m_s}{2} + \frac{f_-}{f_+}\left(\ell + \frac{1}{2}\right)\right). \tag{2}$$

The shifts (50 and 130 mHz per cyclotron quantum and spin flip) arise from a saturated iron ring [Fig. 2(a)] that adds (to $\mathbf{B}$) a magnetic bottle gradient (at the trap center),

$$\Delta\mathbf{B} = \beta_2[(z^2 - \rho^2/2)\hat{\mathbf{z}} - z\rho\hat{\boldsymbol{\rho}}]. \tag{3}$$

The effective f_z shifts because the electrostatic axial oscillator Hamiltonian going as $f_z^2 z^2$ acquires μz^2 from the interaction of the cyclotron, magnetron, and spin moments, $\mu\hat{\mathbf{z}}$, with $\Delta\mathbf{B}$. The bottle strength, $\beta_2 = 2.9 \times 10^5$ T/m^2, is 190 times that used to detect electron spin flips [5] to compensate partially for the small μ_N.

The $\bar{p}$ are transferred between the analysis trap and an adjacent coaxial trap (not in Fig. 2) by slowly varying the applied electrode voltages to make the axial potential well move adiabatically between the two trap centers. In the adjacent trap the $\bar{p}$ cyclotron motion induces currents in and comes to thermal equilibrium with an attached damping circuit cooled with the trap. The cooled $\bar{p}$ is transferred back to the analysis trap and a measured shift $\Delta f_z <$ 100 Hz is required to ensure a cyclotron radius below 0.7 μm (a bit larger than was possible with more time in Ref. [6]) before measuring f_s. For larger shifts, the $\bar{p}$ is returned to the precision trap for cyclotron damping as needed until a low cyclotron energy is selected.

Two methods are used to measure the Δf_z of Eq. (2) in the analysis trap, though the choice of which method to use in which context is more historical than necessary at the current precision. The first (used to detect cyclotron transitions with the weakest possible driving force) takes Δf_z to be the shift of the frequency at which Johnson noise in a detection circuit is canceled by the signal from the $\bar{p}$ axial motion that it drives [14]. The second (used to detect spin flips) takes Δf_z to be the shift of the frequency of a

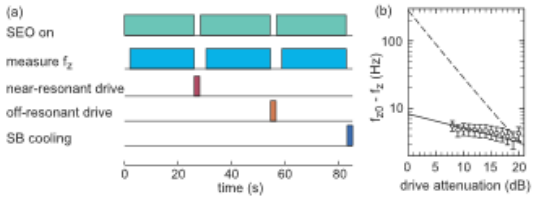

FIG. 3 (color online). (a) Spin measurement cycle. (b) The power shift in f_z due to the spin flip drive (points) is lower than was observed for the proton measurement with no transmission line transformer (dashes).

self-excited oscillator (SEO) [7]. The SEO oscillation arises when the amplified signal from the $\bar{p}$ axial oscillation is fed back to drive the $\bar{p}$ into a steady state.

The measurement cycle in Fig. 3 is used to find the spin resonance. After the SEO stabilizes for 2 s, its frequency average over 24 seconds is f_1. With the SEO off, a nearly resonant spin flip drive at frequency f_d is applied for 2 s. After the SEO is back on for 2 s, the average frequency f_2 is measured to determine the deviation $\Delta = f_2 - f_1$. A spin drive detuned 100 kHz from resonance is next applied with the SEO off—detuned rather than off to control for possible secondary frequency shifts due to the drive. The average f_3 is then measured and compared to f_2. The cycle concludes with 2 s of sideband cooling to prevent magnetron radius growth [7].

Repeating the measurement cycle yields a sequence of deviations Δ_i that can be characterized by an Allen variance $\sigma^2 = \sum_{i=1}^{N} \Delta_i^2/(2N)$ (often used to describe the stability of frequency sources). Even when no spin drive is applied, jitter in the axial frequency (not well understood [7]) gives the Allan variance a nonzero value σ_0^2 comparable to the deviation caused by a spin flip. This jitter increases with cyclotron radius so σ_0^2 is reduced by selecting a $\bar{p}$ with small cyclotron radius (as described earlier). When a drive at frequency $f_d \approx f_s$ induces spin flips, the Allan variance increases slightly to $\sigma_f^2 = \sigma_0^2 + \sigma^2$.

Both the spin and cyclotron resonances are expected to show no excitation until the drive frequency increases above a sharp threshold [13,15]. The driving force has no effect below a resonance frequency (f_+ or f_s here). The transition rate between quantum states and the resulting broadening increases abruptly to its maximum at the resonant frequency. Above this threshold there is a distribution of cyclotron or spin frequencies at which these motions can be driven. These correspond to the distribution of B sampled by the thermal axial motion of the $\bar{p}$ (in thermal equilibrium with the axial detection circuit) within the magnetic bottle gradient.

The spin and cyclotron motions are not damped in the analysis trap so the natural linewidth does not broaden the sharp threshold edges. The superconducting solenoid produces a stable B that does not significantly broaden the edge. A small broadening arising because sideband cooling (of magnetron motion coupled to axial motion) selects different values from a distribution of magnetron radii (explored in detail in Ref. [7]) is added as "magnetron broadening" uncertainty in Table I.

TABLE I. Significant uncertainties in ppm.

Resonance	Source	ppm
Spin	Resonance frequency	2.7
Spin	Magnetron broadening	1.3
Cyclotron	Resonance frequency	3.2
Cyclotron	Magnetron broadening	0.7
Total		4.4

For each drive frequency in Fig. 4(a) the cycle in Fig. 3 is repeated for 24 to 48 hours. The Allan deviation σ_f for the sequence of deviations $\Delta_f = f_2 - f_1$ represents the effect of fluctuations when a near-resonant spin drive is applied. The Allan deviation σ_0 for the sequence of deviations $\Delta_0 = f_3 - f_2$ represents fluctuations when no near-resonant drive is applied. The spin line shape in Fig. 4(a) shows $\sigma^2 = \sigma_f^2 - \sigma_0^2$ vs drive frequency. The scale to the right in Fig. 4(a) is the average probability that the spin drive pulse makes a spin flip.

Matching a 221 MHz drive so that the oscillating current divides equally between the two sides of an electrode [Fig. 2(c)] within a cryogenic vacuum enclosure is challenging, but is improved with a transmission line transformer for this measurement. The drive applied still observably shifts f_z as a function of spin drive power [Fig. 3(b)], presumably because the average trapping potential is slightly modified, but less than for the p measurement. The shift from the strongest drive in Fig. 3(b) is too small to contribute to the measurement uncertainty.

The basic idea of the cyclotron frequency measurement is much the same as for the spin frequency. The applied resonant drive is weak enough to cause no detectable growth in the average cyclotron radius and energy, but strong enough to increase the measured Allan variance σ_f^2. The cyclotron line shape [Fig. 4(b)] shows the expected sharp threshold at the trap cyclotron frequency f_+.

For each of the drive frequencies represented in the cyclotron line shape in Fig. 4(b) a cyclotron drive is applied continuously for 2 to 4 hours. Deviations Δ_i between

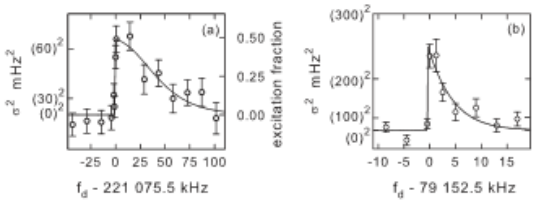

FIG. 4. (a) The spin line. (b) The cyclotron line.

consecutive 80 s f_z averages are characterized by an Allan variance σ_f^2. Then σ_0^2 (from below the threshold frequency) is subtracted to get σ^2.

No fits to expected resonance line shapes are used for this measurement, but the spin line shape fits well to the Brownian motion line shape [15] expected for magnetic field fluctuations caused by thermal axial motion within a magnetic bottle gradient for a spin 1/2 system. An axial temperature of 8 K is extracted from the fit, consistent with measurements using a magnetron method detailed in Ref. [7]. With no expected line shape yet available for the cyclotron resonance, we note that the cyclotron line fits well to the expected spin line shape but with an axial temperature of 4 K. A proper diffusion treatment of the way that a cyclotron drive moves the population between cyclotron states is still needed.

A ratio of frequencies determines the magnetic moment in nuclear magnetons [Eq. (1)]. The free space cyclotron frequency, $f_c = eB/(2\pi m_p)$, is needed while the trap eigenfrequencies f_+, f_z, and f_- are measured directly. The Brown-Gabrielse invariance theorem, $f_c^2 = f_+^2 + f_z^2 + f_-^2$ [16] determines f_c from the eigenfrequencies of an (unavoidably) imperfect Penning trap.

Applying Eq. (1) gives the measured $\bar{p}$ magnetic moment

$$\mu_{\bar{p}}/\mu_N = -2.792\,845 \pm 0.000\,012 \quad [4.4\ \text{ppm}]. \quad (4)$$

The total uncertainty, with all known contributions detailed in Table I is 680 times smaller than obtained in an exotic atom measurement. Frequency uncertainties are the half widths of the sharp edges in the line shapes, determined less precisely than for μ_p because larger frequency steps were taken. The magnetron linewidth uncertainty comes from the distribution of magnetron radii following sideband cooling done without and with simultaneous axial feedback cooling [7,17] for the spin and cyclotron cases. Comparing $\mu_{\bar{p}}$ to previously measured μ_p gives

$$\mu_{\bar{p}}/\mu_p = -1.000\,000 \pm 0.000\,005 \quad [5.1\ \text{ppm}], \quad (5)$$

$$\mu_{\bar{p}}/\mu_p = -0.9999992 \pm 0.0000044 \quad [4.4\,\text{ppm}], \quad (6)$$

consistent with the prediction of the *CPT* theorem. The first uses the μ_p directly measured within the same trap electrodes [6]. The second uses the more precise μ_p deduced indirectly from three measurements (not possible with $\bar{p}$) and two theoretical corrections [18,19].

A comparison of the $\bar{p}$ and p moments that is 10^3 to 10^4 times more precise seems feasible, to make a baryon *CPT* test with a precision approaching the 9×10^{-11} comparison of the charge-to-mass ratios of $\bar{p}$ and p [2]. Individual spin flips must be resolved so quantum jump spectroscopy can be used to measure f_s, as done to measure the electron magnetic moment [5]. The jitter of f_z described above is the challenge since this is not much than the shift from a spin flip. So far, in just one measurement cycle, we can already determine the spin state with a fidelity above 0.95 in about 1 of 4 attempts [20] but are hopeful that this efficiency can be improved (with adiabatic passage or π pulse methods) to allow making a spin resonance in a reasonable time. The magnetic gradient used to detect an electron spin flip was small enough that flipping and detecting the spin could be done in the same trap. To avoid the line broadening due to the large magnetic gradient needed to detect a $\bar{p}$ spin state, spin flips must be driven in an adjacent trap with no magnetic gradient before being transferred to the trap used for spin state detection (as done with ions [21]). Measuring the cyclotron frequency f_c, the second frequency needed to determine the $\bar{p}$ magnetic moment, has already been demonstrated to better than 10^{-10} [2] in a trap with essentially no magnetic gradient.

In conclusion, a direct measurement of the $\bar{p}$ magnetic moment to 4.4 ppm is made with a single $\bar{p}$ suspended in a Penning trap, improving upon the value from exotic atom spectroscopy by a factor of 680. The measured ratio of the $\bar{p}$ and p magnetic moments is consistent with the value of -1 predicted by the *CPT* theorem to 5 ppm or better. It seems possible in the future to compare the magnetic moments of $\bar{p}$ and p more precisely, by a factor of 10^3 or 10^4 in addition to what is reported here.

Thanks to CERN for the 5-MeV $\bar{p}$ and some support for W. O, and to N. Jones for helpful comments. This work was supported by the U.S. NSF and AFOSR, and the Canadian NSERC, CRC, and CFI.

*ATRAP Collaboration Spokesperson.
gabrielse@physics.harvard.edu

[1] G. Lüders, Ann. Phys. (N.Y.) **2**, 1 (1957).
[2] G. Gabrielse, A. Khabbaz, D. S. Hall, C. Heimann, H. Kalinowsky, and W. Jhe, Phys. Rev. Lett. **82**, 3198 (1999).
[3] A. Kreissl, A. Hancock, H. Koch, T. Köehler, H. Poth, U. Raich, D. Rohmann, A. Wolf, L. Tauscher, A. Nilsson, M. Suffert, M. Chardalas, S. Dedoussis, H. Daniel, T. von Egidy, F. Hartmann, W. Kanert, H. Plendl, G. Schmidt, and J. Reidy, Z. Phys. C **37**, 557 (1988).
[4] T. Pask, D. Barna, A. Dax, R. Hayano, M. Hori, D. Horváth, S. Friedrich, B. Juhsz, O. Massiczek, N. Ono, A. Sótér, and E. Widmann, Phys. Lett. B **678**, 55 (2009).
[5] D. Hanneke, S. Fogwell, and G. Gabrielse, Phys. Rev. Lett. **100**, 120801 (2008).
[6] J. DiSciacca and G. Gabrielse, Phys. Rev. Lett. **108**, 153001 (2012), Note the following correction: an observed Δf_z of 20 Hz rather than 50 Hz signaled a 0.3 μm cyclotron radius.
[7] N. Guise, J. DiSciacca, and G. Gabrielse, Phys. Rev. Lett. **104**, 143001 (2010).
[8] S. Ulmer, C. C. Rodegheri, K. Blaum, H. Kracke, A. Mooser, W. Quint, and J. Walz, Phys. Rev. Lett. **106**, 253001 (2011).
[9] C. C. Rodegheri, K. Blaum, H. Kracke, S. Kreim, A. Mooser, W. Quint, S. Ulmer, and J. Walz, New J. Phys. **14**, 063011 (2012).

[10] G. Gabrielse, X. Fei, L. A. Orozco, R. L. Tjoelker, J. Haas, H. Kalinowsky, T. A. Trainor, and W. Kells, Phys. Rev. Lett. **65**, 1317 (1990).
[11] G. Gabrielse, L. Haarsma, and S. L. Rolston, Int. J. Mass Spectrom. Ion Process. **88**, 319 (1989); **93**, 121 (1989).
[12] G. Gabrielse, Adv. At. Mol. Opt. Phys. **45**, 1 (2001).
[13] L. S. Brown and G. Gabrielse, Rev. Mod. Phys. **58**, 233 (1986).
[14] H. Dehmelt and F. Walls, Phys. Rev. Lett. **21**, 127 (1968).
[15] L. S. Brown, Ann. Phys. (N.Y.) **159**, 62 (1985).
[16] L. S. Brown and G. Gabrielse, Phys. Rev. A **25**, 2423 (1982).
[17] B. D'Urso, B. Odom, and G. Gabrielse, Phys. Rev. Lett. **90**, 043001 (2003).
[18] P. Winkler, D. Kleppner, T. Myint, and F. Walther, Phys. Rev. A **5**, 83 (1972).
[19] P. J. Mohr and B. N. Taylor, Rev. Mod. Phys. **72**, 351 (2000).
[20] J. DiSciacca *et al.* (to be published).
[21] H. Häffner, T. Beier, S. Djekić, N. Hermanspahn, H.-J. Kluge, W. Quint, S. Stahl, J. Verdú, T. Valenzuela, and G. Werth, Eur. Phys. J. D **22**, 163 (2003).

Resolving an Individual One-Proton Spin Flip to Determine a Proton Spin State

J. DiSciacca, M. Marshall, K. Marable, and G. Gabrielse*

Department of Physics, Harvard University, Cambridge, Massachusetts 02138, USA

(Received 21 February 2013; published 4 April 2013)

Previous measurements with a single trapped proton (p) or antiproton ($\bar{p}$) detected spin resonance from the increased scatter of frequency measurements caused by many spin flips. Here a measured correlation confirms that individual spin transitions and states are rapidly detected instead. The 96% fidelity and an efficiency expected to approach unity suggests that it may be possible to use quantum jump spectroscopy to measure the p and $\bar{p}$ magnetic moments much more precisely.

DOI: 10.1103/PhysRevLett.110.140406 PACS numbers: 13.40.Em, 14.20.Dh, 37.10.Ty

The fundamental reason for the striking imbalance of matter and antimatter in the Universe has yet to be discovered. Precise comparisons of antimatter and matter particles are thus of interest. Within the standard model of particle physics, a *CPT* theorem [1] predicts the relative properties of particles and antiparticles. (The initials represent charge conjugation, parity, and time reversal symmetry transformations.) The theorem pertains because systems are described by using local, Lorentz-invariant quantum field theory. Whether the *CPT* theorem is universal, of course, is open to question, since gravity so far eludes a quantum field theory description. A testable prediction is that particles and antiparticles have magnetic moments of the same magnitude and opposite sign. The moment of a single trapped $\bar{p}$ [2] was recently measured to a precision 680 times higher than had been possible with other methods. The ratio of $\bar{p}$ and p moments is consistent with the *CPT* prediction to 4.4 ppm.

Quantum jump spectroscopy of a single trapped electron shows that a magnetic moment can be measured much more precisely, to 3 parts in 10^{13} [3]. Individual spin transitions were resolved to determine the needed spin precession frequency. For the substantially smaller nuclear moments of the $\bar{p}$ and p, this is much more difficult. This Letter reports the first observation of individual spin transitions and states for a single p in a Penning trap, with a method applicable for a $\bar{p}$. A high 96% fidelity is realized by selecting a low energy cyclotron motion from a thermal distribution, by saturating the spin transition, and by careful radio frequency shielding. The modest spin state detection efficiency realized in this initial demonstration could be used to make a magnetic moment measurement. However, it now seems possible to use adiabatic passage to detect the spin state in every detection attempt to decrease the measurement time. The possibility to measure a $\bar{p}$ cyclotron frequency (the other frequency needed to determine the moment) has been demonstrated to better than 1 part in 10^{10} [4] to compare the charge-to-mass ratios of the $\bar{p}$ and p [4]. With the spin method demonstrated here, it may be possible to approach this precision in comparing the $\bar{p}$ and p magnetic moments to make a second precise test of the *CPT* theorem with a baryon.

The trap electrodes in Fig. 1 have already been used with both a p and a $\bar{p}$. They were used in 2011 to measure the p magnetic moment [5], in early 2012 for this p demonstration, and then in mid-2012 were moved to CERN to measure the $\bar{p}$ magnetic moment [2]. Leaving details to the other reports, the p is suspended at the center of an iron ring electrode sandwiched between OFE copper electrodes. The electrodes have gold evaporated on their surfaces. Thermal contact with liquid helium keeps them at 4.2 K and gives a vacuum that essentially eliminates collisions with background gas atoms. Voltages applied to electrodes with a carefully chosen relative geometry [6] give a high quality electrostatic quadrupole potential while allowing the proton to be moved into the trap through the open access from either end.

In a magnetic field $\mathbf{B} \approx -5\hat{\mathbf{z}}$ T [vertical in Fig. 1(a)], the proton's spin up and down energy levels are separated by hf_s, with a spin precession frequency $f_s = 221.35$ MHz. The proton energy in the magnetic field is higher for a spin that is up with respect to the quantization

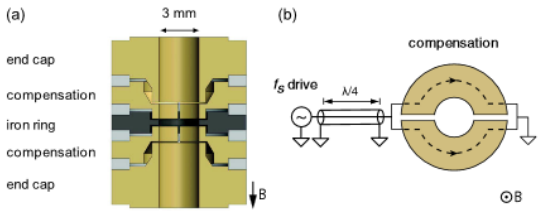

FIG. 1 (color online). (a) Cutaway side view of Penning trap electrodes. All are copper except for an iron ring that makes the magnetic gradient needed to observe a spin flip. (b) Top view of the oscillating current paths for the spin flip drive.

axis $\hat{\mathbf{z}}$ than for a spin down. A driving force that can flip the spin involves a magnetic field perpendicular to $\mathbf{B}$ that oscillates at approximately f_s. This field is generated by currents sent through halves of a compensation electrode [Fig. 1(b)]. The trapped proton's circular cyclotron motion is perpendicular to $\mathbf{B}$ with a frequency $f_+ = 79.26$ MHz slightly shifted from f_c by the electrostatic potential. The proton also oscillates parallel to $\mathbf{B}$ at about $f_z = 919$ kHz. The proton's third motion is a circular magnetron motion, also perpendicular to $\mathbf{B}$, at the much lower frequency $f_- = 5.28$ kHz.

Small measured shifts in the axial frequency f_z,

$$\Delta f_z \propto \left(n + \frac{1}{2} + \frac{g_p m_s}{2} + \frac{f_-}{f_+}\left[\ell + \frac{1}{2}\right]\right), \quad (1)$$

reveal changes in the cyclotron, spin, and magnetron quantum numbers n, m_s, and ℓ, respectively [7]. The shifts are taken to be the shifts in the self-excited oscillation (SEO) that arises when amplified signal from the proton's axial oscillation is fed back to drive the p into a steady-state oscillation [8]. The shifts arise as the magnetic moments of these motions interact with a magnetic bottle gradient from the saturated iron ring,

$$\Delta \mathbf{B} = \beta_2[(z^2 - \rho^2/2)\hat{\mathbf{z}} - z\rho\hat{\boldsymbol{\rho}}], \quad (2)$$

with $\beta_2 = 2.9 \times 10^5$ T/m^2. A spin flip causes only a tiny shift, $\Delta_s = 130$ mHz, despite the gradient being 190 times larger than used to detect electron spin flips [3], because a nuclear moment is smaller than an electron moment by of the order of $1/2000$, the ratio of the electron and proton masses.

Counting individual spin flips for quantum jump spectroscopy requires identifying the small shifts $\pm\Delta_s$. The nearly 15 h of f_z measurements in Fig. 2(a) illustrate

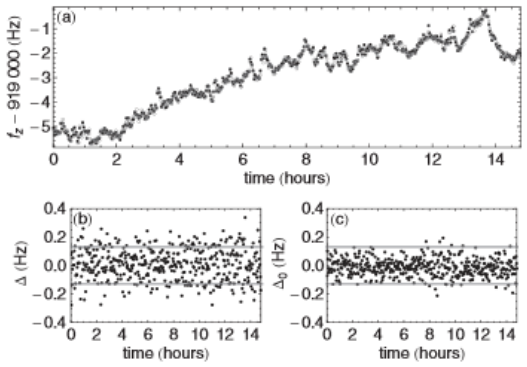

FIG. 2. (a) Repeated measurements of f_z show a large drift and scatter. (b) Scatter in the measured frequency shifts Δ for a resonant spin drive has $\sigma = 109$ mHz. (c) Scatter in the measured frequency shifts Δ_0 for an off-resonant spin drive that causes no spin flips has $\sigma_0 = 63$ mHz. The gray lines show the spin flip shift $\pm\Delta_s$.

the challenge of observing such small shifts despite much larger frequency drifts and fluctuations. Repeated applications of a detection cycle (Fig. 3) yield a series of frequency shifts $\Delta = f_2 - f_1$ that take place for a resonant spin drive [Fig. 2(b)] and a series of shifts $\Delta_0 = f_3 - f_2$ for a nonresonant spin drive [Fig. 2(c)]. The f_i are averages of the SEO frequency for three 32 s periods. In the 4 s intervals between the averaging periods, the SEO is off and either a resonant or nonresonant (detuned 100 kHz) spin flip drive is applied for the first 2 s.

The detection cycle concludes with 2 s of sideband cooling and feedback cooling that prevents the average magnetron radius from growing. Each cooling application, however, establishes a slightly different magnetron radius that cannot be predicted [8], adding here a 122 ± 5 mHz spread of f_z values that is comparable to Δ_s.

The distribution of fluctuations Δ_0 observed without spin flips [the gray histogram in Fig. 4(a) derived from Fig. 2(c)] fits well to a normalized Gaussian probability function $G(\Delta_0, \sigma_0)$ with a standard deviation $\sigma_0 = 63$ mHz. This is significantly smaller than the 112 and 145 mHz for the p and $\bar{p}$ measurements [2,5]. (The Allen deviation used in Refs. [2,5] is smaller by $\sqrt{2}$.) Though Δ_0 is larger than we would like, a distribution this narrow requires a p with an unusually small cyclotron orbit, since the fluctuations are observed to increase linearly with cyclotron radius [5]. A p is repeatedly transferred between the trap of Fig. 1 and a coaxial trap whose attached circuit damps the cyclotron motion, until a p with a cyclotron energy below the thermal average is selected. Reducing σ_0 is complicated, because the causes of the fluctuations are difficult to identify and control [8]. One candidate is noise that makes it past considerable radio frequency shielding to drive the cyclotron motion, with a single quantum change shifting f_z by 50 mHz.

We can predict the distribution of shifts Δ for a long series of detection cycles when the resonant spin drive is strong enough to saturate the spin transition. Half of the detection cycles should produce no spin flip and thus have a distribution of Δ given by $G(\Delta, \sigma_0)/2$. A quarter each of the detection cycles should involve spin up and spin down transitions described by $G(\Delta \mp \Delta_s, \sigma_0)/4$, since the spin

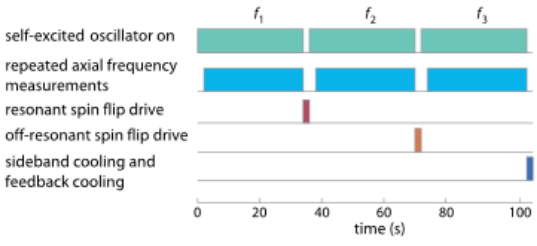

FIG. 3 (color online). Spin detection cycle repeated nearly 15 h.

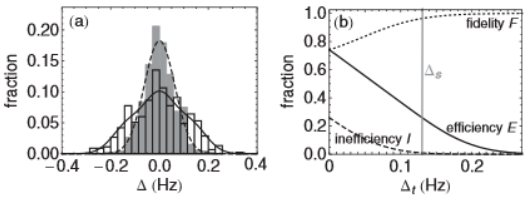

FIG. 4. (a) The gray histogram of measured changes Δ_0 with no spin flip drive fit well to a Gaussian (dashed curve). The predicted histogram shape for a resonant drive that saturates the spin transition (solid curve), and the measured open histogram. (b) E, I, and F for a detection cycle that employs a resonant spin drive that saturates the spin transition.

changes add shifts $\pm\Delta_s$ to the random fluctuations Δ_0 observed when no spin is flipped.

The sum of the three predicted distributions is the solid curve in Fig. 4(a). Our interpretation is supported by the good agreement with the open histogram in Fig. 4(a) derived from the observed Δ in Fig. 2(b). The observed standard deviation has a $\sigma = 109$ mHz, clearly larger than σ_0 for the gray histogram for no spin flips. For the $\bar{p}$ magnetic moment measurement [2] and related p studies [5,9,10], the increase from σ_0 to σ is used to find spin resonance with no individual spin flip being resolved. Here, encouraged by the good agreement of the prediction and the observation, we first argue that we are able to identify spin flips from the individual Δ values in Fig. 2(b) and then confirm this assertion by using a measured spin correlation function.

Each Δ would unambiguously reveal which spin flip had occurred, if any, if the Δ_0 for the off-resonance drive fluctuated much less than the spin flip shift Δ_s, so $\sigma_0 \ll \Delta_s$. In this limit the open histogram would be three resolved histograms, each with a width characterized by σ_0. The much larger electron magnetic moment makes this possible for measuring the electron moment [3].

More care is required for p and $\bar{p}$. Since $\sigma_0 = 63$ mHz is only half of $\Delta_s = 130$ mHz, some fluctuations will be able to hide whether a spin flip shift $\pm\Delta_s$ has taken place. For a detection cycle that flips the spin state with probability P, the four ways to produce an above-threshold $\Delta \geq \Delta_t$ for positive $\Delta_t > 0$ have probabilities

$$P_{\Uparrow\Uparrow}(\Delta_t) = P\int_{\Delta_t}^{\infty} G(\Delta - \Delta_s, \sigma_0)d\Delta, \quad (3)$$

$$P_{\Uparrow\Downarrow}(\Delta_t) = P_{\Downarrow\Uparrow}(\Delta_t) = (1-P)\int_{\Delta_t}^{\infty} G(\Delta, \sigma_0)d\Delta, \quad (4)$$

$$P_{\Downarrow\Downarrow}(\Delta_t) = P\int_{\Delta_t}^{\infty} G(\Delta + \Delta_s, \sigma_0)d\Delta. \quad (5)$$

The largest, $P_{\Uparrow\Uparrow}(\Delta_t)$, is for a detection cycle that flips the spin from down to up. The probabilities $P_{\Uparrow\Downarrow}(\Delta_t) = P_{\Downarrow\Uparrow}(\Delta_t)$ are smaller, and $P_{\Downarrow\Downarrow}(\Delta_t)$ is smaller still.

A detection cycle produces an above-threshold shift $\Delta \geq \Delta_t$ with an efficiency E for a spin that is down before the cycle begins, and with an efficiency I for a spin that is instead up before the cycle begins, with

$$E = P_{\Uparrow\Uparrow}(\Delta_t) + P_{\Downarrow\Uparrow}(\Delta_t), \quad (6)$$

$$I = P_{\Uparrow\Downarrow}(\Delta_t) + P_{\Downarrow\Downarrow}(\Delta_t). \quad (7)$$

The latter is thus an inefficiency with respect to detecting a spin that was initially down. The fidelity $F = E/(E + I)$ represents the reliability with which we determine the spin state. It is the fraction of above-threshold events that result from a spin that starts down when the detection cycle is applied. The same values of E, I, and F pertain for "above"-threshold events $\Delta \leq -\Delta_t$ observed when a single detection cycle is applied to a spin up.

The dependence of E, I, and F upon the choice of threshold Δ_t is shown in Fig. 4(b) for a resonant drive that saturates the spin transition (i.e., $P = 1/2$), along with our Δ_s and σ_0. Choosing a threshold equal to the spin flip shift, $\Delta_t = \Delta_s$, gives a high fidelity $F = 96\%$ and a low $I = 1\%$. However, the efficiency $E = 26\%$ means that a spin down will produce an above-threshold event that establishes the spin state with this high fidelity about in 1 in 4 attempts. Roughly speaking, half of the detection cycles flip the spin as needed to get an above-threshold event, and half of these cycles have fluctuations of the same sign as the spin flip shift. If a lower fidelity suffices the efficiency is much higher, with $F = 88\%$ giving $E = 48\%$, for example.

A 3 h slice of Δ measurements [from Fig. 2(b)] is shown in Fig. 5(a). Below, in Fig. 5(b), are spin state determinations (at the end of the detection cycles) made by using a threshold $\Delta_t = \Delta_s$ to get a fidelity of 96% for about 1 in 4 detection cycles.

A nearly perfect detection efficiency (with the spin state determined in each detection cycle rather than in 1 of 4 for

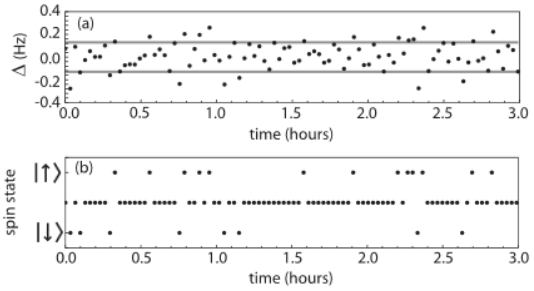

FIG. 5. (a) Three hour sample of frequency shifts Δ [from Fig. 2(b)]. (b) Corresponding identifications of the spin state based upon above-threshold Δ for a threshold of $\Delta_t = \Delta_s$. Points between the heights of the identified spin states indicate that no spin state identification could be made with this threshold choice.

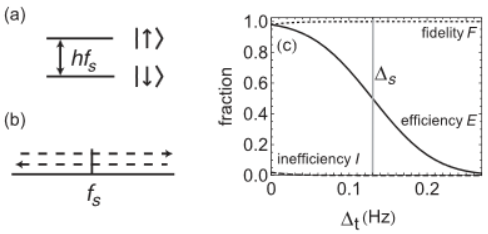

FIG. 6. (a) Spin energy levels. (b) For adiabatic passage the drive frequency is swept adiabatically upward or downward through resonance. (c) The efficiency E, inefficiency I, and fidelity F for an adiabatic passage spin drive applied during the detection cycle.

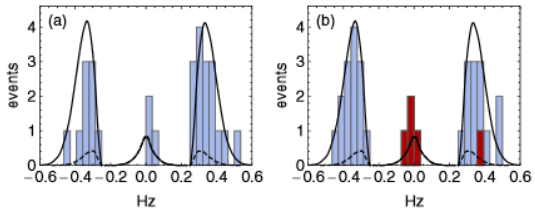

FIG. 7 (color online). The solid curve is the predicted shape of the correlation histogram for adjacent above-threshold events, and the dashed curve is the predicted distribution of accidentals. The histogram for the 450 detection cycles in our data set (a) agrees qualitatively and quantitatively with our predictions. The histogram in (b) is a simulation for 450 detection cycles. The five accidentals are highlighted.

this simple first demonstration) should be possible with an enhanced detection cycle. We propose to substitute an adiabatic passage drive (or a less robust π pulse) for the simple resonant drive to increase the spin flip probability from $P = 1/2$ to $P = 1$. No reduction in $\sigma_0 = 63$ mHz is required. As demonstrated decades ago in NMR measurements, complete population transfer from one state to the other in Fig. 6(a) can be accomplished by sweeping the drive adiabatically either upwards or downwards through resonance [Fig. 6(b)]. Figure 6(c) shows how the fidelity and efficiency depend on threshold. A threshold of $\Delta_t = 0$ mHz, for example, gives a nearly perfect fidelity $F = 98\%$ and efficiency $E = 98\%$. The care that must be taken to minimize the possible disruption of population transfer from thermal axial motion in the magnetic gradient is under study.

Confirming evidence that individual spin flips are being observed comes from a measured correlation function [Fig. 7(a)] that is qualitatively and quantitatively consistent with predictions. We use correlations $\Delta_2 - \Delta_1$ that come from a detection cycle that produces an above-threshold Δ_1, followed immediately by a second detection cycle that also produces an above-threshold Δ_2. For the 450 detection cycles of our data set, with the observed $\sigma_0 = 63$ mHz and chosen threshold $\Delta_t = \Delta_s$, there are about $E\,450 \approx 120$ above-threshold Δ (with either $\Delta \geq \Delta_t$ or $\Delta \leq -\Delta_t$). About $E^2\,450 \approx 30$ pairs of these are produced by sequential detection cycles and thus contribute to Fig. 7(a).

Qualitatively, a histogram of these correlations should have half of its entries below $-2\Delta_s$ (for a spin that flips from up to down in the first cycle and from down to up in the next). The other half of the entries should be in a peak above $2\Delta_s$ (for a spin that flips from down to up in the first cycle and from up to down in the next). Ideally, there should be no entries between the peaks, since correlations near zero would require a spin to switch from either up to down or down to up in both of the cycles, and this is not possible. However, because the fidelity is not perfect, some accidentals are expected between the peaks and elsewhere. These are entries for which one or both of the above-threshold events is due to unusually large fluctuations rather than from a spin flip.

Quantitative predictions come from simulations. The solid curve in Fig. 7 gives the predicted shapes of the correlation histogram for the measured σ_0 and a threshold choice $\Delta_t = \Delta_s$. The dashed curve, the predicted distribution of accidentals, shows that the small central peak is entirely from accidentals, since for this peak the solid and dashed curves overlap.

The measured correlation histogram in Fig. 7(a) for the 450 detection cycles of our data set agrees well with the prediction. It has 25 counts in the side peaks and 3 in the center, consistent with the predicted 30 ± 7 in the side peaks (with 2 ± 2 of these from accidentals) along with 2 ± 2 in the central peak from accidentals.

Figure 7(b) shows one of many simulated correlation histograms for 450 detection cycles, with five accidentals highlighted to distinguish them. From many such trials we get the mean number and uncertainty for the number of counts in each peak and for the number of accidentals.

In conclusion, the correlation histogram adds convincing evidence that individual proton spin flips are being observed and well understood. Individual spin flips of a single trapped proton are observed as above-threshold frequency shifts produced by using a detection cycle that employs the simplest saturated spin drive. The 96% fidelity achieved in this first demonstration makes it possible to identify the spin state for 1 in 4 detection cycles. A nearly perfect efficiency is predicted when an adiabatic passage drive is substituted for the resonant drive in the detection cycle. The observations of individual, single proton spin flips open the possibility of quantum jump spectroscopy measurement of the spin frequency for a $\bar{p}$ or p, to go with precise measurements of their cyclotron frequency demonstrated earlier. It may eventually be possible to measure these frequencies precisely enough to determine the proton and antiproton magnetic moments a factor of 10^3–10^4 times more precisely than achieved in the

recent measurement of the $\bar{p}$ magnetic moment—itself a 680-fold improvement in precision compared to previous measurements.

Thanks to the NSF AMO program and the AFOSR for support and to S. Ettenauer and E. Tardiff for helpful comments on the manuscript.

Note added.—Related observations are discussed in Ref. [11].

*gabrielse@physics.harvard.edu

[1] G. Lüders, Ann. Phys. (N.Y.) **2**, 1 (1957).
[2] J. DiSciacca *et al.* (ATRAP Collaboration), Phys. Rev. Lett. **110**, 130801 (2013).
[3] D. Hanneke, S. Fogwell, and G. Gabrielse, Phys. Rev. Lett. **100**, 120801 (2008).
[4] G. Gabrielse, A. Khabbaz, D. S. Hall, C. Heimann, H. Kalinowsky, and W. Jhe, Phys. Rev. Lett. **82**, 3198 (1999).
[5] J. DiSciacca and G. Gabrielse, Phys. Rev. Lett. **108**, 153001 (2012).
[6] G. Gabrielse, L. Haarsma, and S. L. Rolston, Int. J. Mass Spectrom. Ion Process. **88**, 319 (1989); **93**, 121 (1989).
[7] L. S. Brown and G. Gabrielse, Rev. Mod. Phys. **58**, 233 (1986).
[8] N. Guise, J. DiSciacca, and G. Gabrielse, Phys. Rev. Lett. **104**, 143001 (2010).
[9] S. Ulmer, C. C. Rodegheri, K. Blaum, H. Kracke, A. Mooser, W. Quint, and J. Walz, Phys. Rev. Lett. **106**, 253001 (2011).
[10] C. C. Rodegheri, K. Blaum, H. Kracke, S. Kreim, A. Mooser, W. Quint, S. Ulmer, and J. Walz, New J. Phys. **14**, 063011 (2012).
[11] A. Mooser *et al.*, preceding Comment, Phys. Rev. Lett. **110**, 140405 (2013).

Using electric fields to prevent mirror-trapped antiprotons in antihydrogen studies

P. Richerme,[1] G. Gabrielse,[1,*] S. Ettenauer,[1] R. Kalra,[1] E. Tardiff,[1] D. W. Fitzakerley,[2] M. C. George,[2] E. A. Hessels,[2] C. H. Storry,[2] M. Weel,[2] A. Müllers,[3] and J. Walz[3]
(ATRAP Collaboration)
[1]*Department of Physics, Harvard University, Cambridge, Massachusetts 02138, USA*
[2]*York University, Department of Physics and Astronomy, Toronto, Ontario, Canada M3J 1P3*
[3]*Institut für Physik, Johannes Gutenberg Universität and Helmholtz Institut Mainz, D-55099 Mainz, Germany*
(Received 24 August 2012; published 25 February 2013)

The signature of trapped antihydrogen ($\overline{\mathrm{H}}$) atoms is the annihilation signal detected when the magnetic trap that confines the atoms is suddenly switched off. This signal would be difficult to distinguish from the annihilation signal of any trapped $\bar{p}$ that is released when the magnetic trap is switched off. This work deduces the large cyclotron energy (>137 eV) required for magnetic trapping of $\bar{p}$, considers the possibility that such $\bar{p}$ are produced, and explores the effectiveness of an electric field applied to clear charged particles from the trapping volume before $\overline{\mathrm{H}}$ detection. No mechanisms are found that can give a $\bar{p}$ such a large cyclotron energy and allow it to mimic an $\overline{\mathrm{H}}$ annihilation. The method used to release $\overline{\mathrm{H}}$ atoms from their magnetic trap without removing the magnetic field gradient that could possibly confine $\bar{p}$ with a high cyclotron energy is also discussed.

DOI: 10.1103/PhysRevA.87.023422 PACS number(s): 37.10.De, 36.10.−k, 41.20.−q, 41.90.+e

I. INTRODUCTION

Antihydrogen atoms have recently been trapped for up to about 1000 s by both the ATRAP and ALPHA Collaborations at CERN [1,2]. ATRAP observed an average of 5 atoms per trial confined for $\geqslant$15 s, while ALPHA trapped approximately 0.7 $\overline{\mathrm{H}}$ atoms per trial for $\geqslant$10 s using smaller numbers of antiprotons ($\bar{p}$) and positrons (e^+). These are important steps towards the proposed use of trapped $\overline{\mathrm{H}}$ atoms [3] for *CPT* tests with precision spectroscopy [4] and for proposed gravitational studies with trapped antimatter atoms [5], though larger numbers of trapped atoms will be required.

The $\overline{\mathrm{H}}$ atoms are confined within the magnetic field minimum of a Ioffe trap [6] to which the magnetic moment of weak-field seeking states of the neutral $\overline{\mathrm{H}}$ atoms are attracted. The trapped $\overline{\mathrm{H}}$ atoms are detected via their annihilations with the surrounding apparatus when the current producing the radial Ioffe fields is switched off. It is important that the signal used to identify and count an $\overline{\mathrm{H}}$ atom is from a trapped atom and not from a trapped $\bar{p}$ that is released at the same time, given that an $\overline{\mathrm{H}}$ and a $\bar{p}$ have the same annihilation signals.

A $\bar{p}$ that is given a large cyclotron energy may have a magnetic moment that is large enough to be captured magnetically. The simplest "mirror trap" in which a $\bar{p}$ with cyclotron energy could be confined is a magnetic field that increases in magnitude to either side of the trap center—just the situation that pertains when the axially symmetric contribution to a Ioffe trap field is turned on. A charged $\bar{p}$ is fixed to the field line around which it has its circular cyclotron orbit, and the magnetic moment is confined axially by the gradient magnetic field. Already some time ago, particles in a mirror trap [7] were used to measure the electron and positron magnetic moments [8], to directly trap e^+ for multispecies plasma experiments [9], and to bunch e^+ [10].

This paper discusses the $\bar{p}$ cyclotron energy needed to mirror trap a $\bar{p}$ in the ATRAP Ioffe trap, considers mechanisms for producing these large energies, and examines the effectiveness of the electric field that is applied to clear away possible mirror-trapped $\bar{p}$ while the $\overline{\mathrm{H}}$ atoms are trapped, before these atoms are detected. We seek (unsuccessfully) to identify processes that can provide a $\bar{p}$ with the cyclotron energy necessary for it to remain mirror-trapped when the clearing field is applied. As an added precaution, the $\overline{\mathrm{H}}$ atoms are released for detection while the mirror trap from the axially symmetric Ioffe field coils is left on. Mirror trapping requires considerably more $\bar{p}$ cyclotron energy in our apparatus compared to another that has been studied [11].

II. TRAPPED $\overline{\mathrm{H}}$ ATOMS

The apparatus used to observe trapped $\overline{\mathrm{H}}$ atoms in their ground state is represented in Fig. 1. The hollow copper cylinders can be biased as Penning trap electrodes to make open-access Penning traps [12] for $\bar{p}$ and e^+. Currents in the Ioffe pinch coils and the Ioffe racetrack coils make a magnetic field minimum that is centered on these coils. The potentials on the electrodes are manipulated such that e^+ and $\bar{p}$ interact to form $\overline{\mathrm{H}}$ atoms at the field minimum.

$\overline{\mathrm{H}}$ formation at this location proceeds via three-body recombination involving a $\bar{p}$ and two e^+ [13,14] within a nested-well potential [Fig. 2(a)]. Virtually all of the atoms formed are "guiding center atoms" [14] that cannot be magnetically trapped. Some of these atoms are observed to form in states with $n \lesssim 50$ [15]. This atom size is just small enough that the e^+ orbit about the $\bar{p}$ is chaotic, opening the possibility of occasional low-field-seeking states that can be trapped [15]. Some of these atoms remain in low-field-seeking states during their cascade to the ground state [1,2], consistent with simulations [16,17].

To be confined an $\overline{\mathrm{H}}$ atom must have a very low kinetic energy. The trap potential energy contours in Fig. 2(b) are for

*gabrielse@physics.harvard.edu

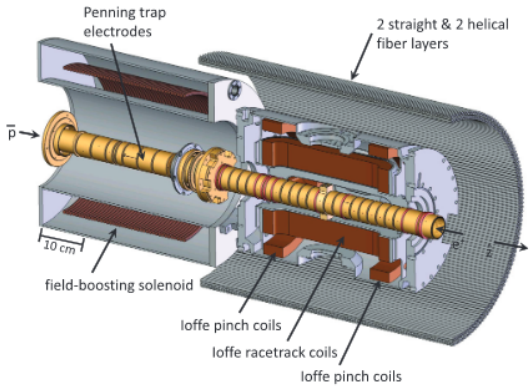

FIG. 1. (Color) Electrodes and coils produce Penning traps (to store $\bar{p}$ and e^+) and a Ioffe trap [6] (to store $\overline{\mathrm{H}}$). Much of the vacuum enclosure and cooling system is hidden to make the traps and detectors visible. An external solenoid (not shown) adds a 1 T magnetic field along the trap axis $\hat{z}$ which is vertical.

a ground-state $\overline{\mathrm{H}}$. The magnetic field on the center axis of the trap is shown in Fig. 2(c).

ATRAP holds trapped $\overline{\mathrm{H}}$ atoms in the Ioffe trap for between 15 and 1000 s (depending upon the method used to make $\bar{p}$ and e^+ interact to form $\overline{\mathrm{H}}$)—long enough for $\overline{\mathrm{H}}$ atoms to decay to their ground state [1]. While the $\overline{\mathrm{H}}$ are trapped, axial electric fields of first +5 V/cm and then −5 V/cm are applied [e.g., the dashed line in Fig. 2(a)], each for 1 s, to force all $\bar{p}$ and e^+

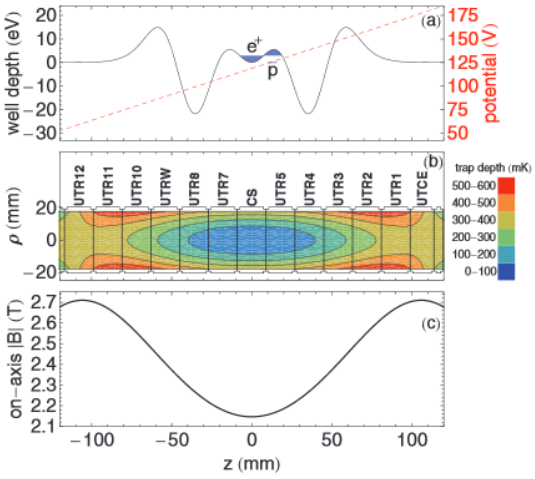

FIG. 2. (Color) (a) Potentials along the center axis of the trap used to contain charged $\bar{p}$ and e^+ until $\overline{\mathrm{H}}$ formation (solid) and remove (dashed) charged particles after $\overline{\mathrm{H}}$ formation. (b) Trap electrode cross sections with equipotential energy contours for a low-field-seeking, ground-state $\overline{\mathrm{H}}$ in the Ioffe trap. (c) The magnitude of the on-axis magnetic field rises from 2.15 T at the center of the trap to 2.71 T near the pinch coils.

to leave the trap. These clearing electric fields are much larger than any stray fields within the Penning trap.

Trapped $\overline{\mathrm{H}}$ atoms leave the trap radially when the current in the Ioffe racetrack coils that produces the radial Ioffe field is switched off. The annihilation signals the $\overline{\mathrm{H}}$ atoms make upon striking electrode surfaces [1] are detected.

III. CYCLOTRON ENERGY NEEDED FOR MIRROR TRAPPING

During $\overline{\mathrm{H}}$ detection, the mirror trap from the Ioffe pinch coils is left on to maximize the chance that a mirror-trapped $\bar{p}$ (if any are present) remains confined. However, possible transient effects upon such $\bar{p}$ from the sudden removal of the radial Ioffe field are not well understood. Thus, it would be better to be confident that no $\bar{p}$ at all were stored in the mirror trap. As a first step this section considers the cyclotron energy needed to produce a magnetic moment large enough to remain trapped when the clearing electric field is applied.

A $\bar{p}$ in the combined fields of a Penning and Ioffe trap executes a modified cyclotron, axial, and magnetron motion compared to its motion in a simple Penning trap [18]. Adiabatic invariants [19] have been identified for each of these motions, provided that the magnetic field changes sufficiently slowly along the $\bar{p}$ trajectory so that orbit frequencies change by only a small fraction during an orbit period, a condition easily satisfied here. For a $\bar{p}$ with cyclotron energy E_c, its magnetic moment $\mu_{\bar{p}} = E_c/|\vec{B}|$ is an adiabatic invariant of the cyclotron motion. As $|\vec{B}|$ increases, E_c also increases to keep $\mu_{\bar{p}}$ fixed.

The sum of the $\bar{p}$ cyclotron energy E_c and the $\bar{p}$ translational kinetic energy E_T also remains fixed. Thus as a $\bar{p}$ moves from a region of weak to strong $|\vec{B}|$, E_c increases to keep $\mu_{\bar{p}}$ invariant, and E_T decreases to keep the total energy constant. If the $\bar{p}$ moves into a $|\vec{B}|$ large enough to reduce the translational energy to $E_T = 0$, the $\bar{p}$ reverses its trajectory and in this sense is "mirror-trapped."

Consider a $\bar{p}$ with kinetic energy E_T and cyclotron energy E_c in a magnetic field, B_0. If the $\bar{p}$ moves to a larger magnetic field B it will not be mirror-trapped if its initial kinetic energy is high enough,

$$E_T > E_c\left(\frac{B}{B_0} - 1\right). \tag{1}$$

The center of the ATRAP Ioffe trap has $B_0 = 2.15$ T and $B_{\max} = 2.71$ T [Fig. 2(c)]. Thus a kinetic energy $E_T > 0.26E_c$ at the trap center ensures that a $\bar{p}$ will not be mirror-trapped. In a $\bar{p}$ plasma with cyclotron and translational motions thermalized at 4 K, an unacceptably large fraction of 8% would be mirror-trapped.

For this reason the strong clearing electric field is introduced to sweep away $\bar{p}$ after $\overline{\mathrm{H}}$ formation. The applied force must be stronger than both the stray fields within the trap electrodes and the mirror-trap restoring force. When a potential Φ is applied, an additional term, $-e\Phi$, must be added to the total energy (where $-e$ is the $\bar{p}$ charge). Equating the total energy at the center of the trap, where $|\vec{B}| = B_0$ and $\Phi = \Phi_0$, to the energy at some other point parametrized by B and Φ, mirror-trapping

is avoided if

$$E_T > E_c\left(\frac{B}{B_0} - 1\right) - e(\Phi - \Phi_0). \quad (2)$$

For large enough $\Phi - \Phi_0$ it is possible to make sure that no $\bar{p}$ is mirror-trapped [i.e., to satisfy Eq. (2)] for any E_c and B, even when $E_T = 0$.

For ATRAP, only a $\bar{p}$ with an extremely high cyclotron energy can remain mirror-trapped after the clearing electric field is applied. Clearing fields of both $+5$ V/cm and -5 V/cm are used [e.g., $+5$ V/cm is the dashed line in Fig. 2(a)] and $(B_{\max}/B_0 - 1) = 0.26$. This means that a minimum cyclotron energy $E_c > 137$ eV is required for a $\bar{p}$ with no translational kinetic energy ($E_c > 200$ eV in the center of the Ioffe trap) to be mirror-trapped. This limit is rather conservative given that a $\bar{p}$ that has no translational energy along a magnetic field line and a high cyclotron energy is very unlikely. Note that since $(B_{\max}/B_0 - 1) = 0.26$ in ATRAP, compared with $(B_{\max}/B_0 - 1) = 1.0$ in the ALPHA apparatus that has been studied [11], we may tolerate a markedly larger value of E_c (137 eV vs. 50 eV) while still satisfying Eq. (2) (for the same E_T and Φ).

Above we have considered only the case of a $\bar{p}$ with no translational energy at the center of the Ioffe trap. Mirror trapping is much less likely in general. To determine whether a $\bar{p}$ with a given E_c at other locations will remain mirror-trapped with the clearing potential applied, we consider first the most restrictive case $E_T = 0$. The right-hand side of Eq. (2) can then be treated as a pseudopotential,

$$V = -e(\Phi - \Phi_0) + E_c\left(\frac{B}{B_0} - 1\right), \quad (3)$$

through which the $\bar{p}$ moves. A $\bar{p}$ remains mirror-trapped only if it stays in a local minimum of the pseudopotential.

The easiest case to visualize is that of a $\bar{p}$ that is on the central axis of the trap since it will stay on this axis. The on-axis potential $\Phi(z)$ is the dashed line in Fig. 2(a), and the on-axis magnetic field strength $B(z)$ is shown in Fig. 2(c). Figure 3(a) shows the on-axis pseudopotential energy as a function of axial position for three values of the cyclotron energy E_c. With a 5 V/cm electric clearing field applied, the pseudopotential contains no local minimum until $E_c > 137$ eV. Thus, any $\bar{p}$ on-axis with $E_c < 137$ eV will be swept away by the clearing potential. Those with $E_c > 137$ eV can remain mirror-trapped but only if they remain spatially localized in the pseudopotential well with too small an energy E_T to escape.

If a $\bar{p}$ on-axis starts with $E_T = 0$ at a higher potential energy far to the left in Fig. 3(a), it may still gain enough kinetic energy to escape over the barrier to the right even if $E_c > 137$ eV. Figure 3(b) plots the minimum cyclotron energy a $\bar{p}$ would need, along with $E_T = 0$, to remain mirror-trapped when starting from different values of z on-axis. The curve reaches a minimum at 137 eV. Away from the minimum, the curve rises to the left on account of the longer distance over which the clearing potential can accelerate $\bar{p}$. The curve rises to the right as $\bar{p}$ are no longer localized in the confining well of the pseudopotential. Note that for $\bar{p}$ located at the center of the nested well ($z = 0$), only those with $E_c > 200$ eV could potentially survive the electric clearing field.

The off-axis trajectories for a $\bar{p}$ in a Penning-Ioffe trap are more complicated due to the presence of the radial Ioffe

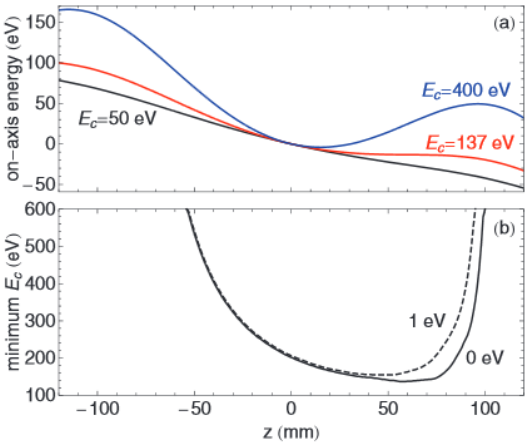

FIG. 3. (Color online) (a) The pseudopotential on-axis is plotted for three different values of $\bar{p}$ cyclotron energy E_c when an electric clearing field of 5 V/cm is applied. At $E_c = 137$ eV, the pseudopotential just begins to show a local minimum. (b) The minimum value E_c a $\bar{p}$ would need to remain mirror-trapped when starting at different axial positions z for $E_T = 0$ and $E_T = 1$ eV and the corresponding pseudopotential in Eq. (3). More cyclotron energy is needed for mirror trapping in some locations for the larger E_T.

field. The magnetic field lines, some of which are shown in Fig. 4(a), are no longer along $\hat{z}$. They diverge exponentially in the planes aligned with the Ioffe current bars (the long vertical sections of the racetrack coils shown in Fig. 1). Nonetheless, the pseudopotential along these field lines may be determined using Eq. (3) with calculated off-axis potentials and the calculated off-axis magnetic field, as illustrated in Fig. 4(b).

To determine if any $\bar{p}$ with $E_c < 137$ eV may be mirror-trapped off-axis, we calculate trajectories for $\bar{p}$ with various E_c and $E_T = 0$ at a grid of starting locations in the trap. To speed

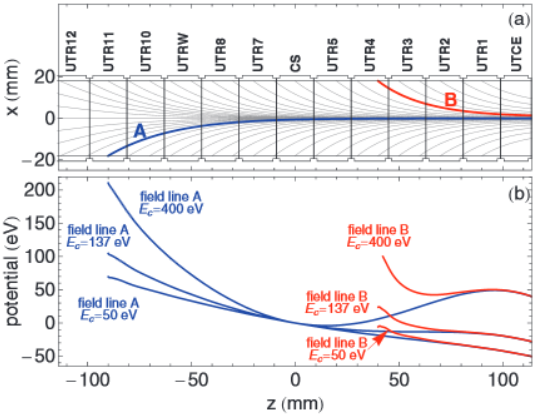

FIG. 4. (Color) (a) A sample of the maximally divergent magnetic field lines in the Penning-Ioffe trap. For various values of E_c, the pseudopotential along the two indicated field lines is plotted in panel (b), projected on the z axis.

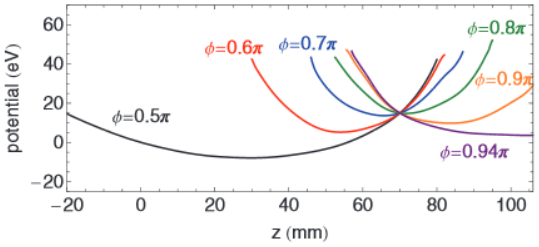

FIG. 5. (Color) The value of the pseudopotential is plotted along magnetic field lines passing through $\rho = 10$ mm, for various ϕ and $z = 70$ mm, for a $\bar{p}$ with $E_c = 200$ eV. Though the $\bar{p}$ may be temporarily mirror-trapped when $\phi = 0.5\pi$, magnetron drift allows the $\bar{p}$ to escape once its azimuthal angle crosses $\phi = 0.94\pi$.

calculations, we employ the guiding-center approximation, in which the fast cyclotron motion is replaced by the adiabatically invariant magnetic moment μ_p that remains aligned with the local magnetic field [20]. Trajectories for $\bar{p}$ off-axis are thus excursions along a magnetic field line with a slight change in azimuthal angle during each bounce due to the magnetron drift.

A $\bar{p}$ will only remain mirror-trapped if it stays in a local minimum of the pseudopotential throughout its entire trajectory. For example, consider a $\bar{p}$ with $E_c = 200$ eV starting at the coordinates $\rho = 10$ mm, $\phi = \pi/2$, and $z = 70$ mm. This $\bar{p}$ will be mirror-trapped initially, as shown in Fig. 5. However, as the $\bar{p}$ magnetron drift changes the azimuthal angle ϕ, the pseudopotential becomes less confining until, at $\phi = 0.94\pi$, the $\bar{p}$ escapes. A $\bar{p}$ is confined in a stable mirror-trapped trajectory if the pseudopotential is confining for all ϕ. Otherwise, the trajectory intersects a trap electrode or exits out the end of the trap.

Figure 6 shows the result of the trajectory calculations. For each of the initial grid locations the minimum initial value of E_c that results in mirror trapping is represented. The lowest cyclotron energy that results in mirror trapping is $E_c = 137$ eV on the trap axis [Fig. 3(b)]. A $\bar{p}$ at any location in the trap will not be mirror-trapped if its initial cyclotron energy is less than 137 eV.

IV. ACQUIRING MORE THAN 137 eV OF CYCLOTRON ENERGY

To minimize the chance that mirror-trapped $\bar{p}$ would be released and counted as $\overline{\mathrm{H}}$ atoms, we do not turn off the axial

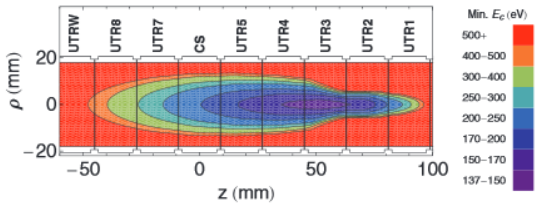

FIG. 6. (Color) The cyclotron energy E_c that a $\bar{p}$ must have at each location in the trap if it is to be mirror-trapped as determined by trajectory calculations. The global minimum, on the center axis of the trap, is $E_c = 137$ eV, so no $\bar{p}$ with $E_c < 137$ eV is mirror-trapped.

mirror trap (from the Ioffe pinch coils of Fig. 1) when releasing trapped $\overline{\mathrm{H}}$ atoms to count them. Instead, only the currents in the Ioffe racetracks (Fig. 1) are switched off. It would be safer, of course, if no $\bar{p}$ was mirror-trapped when the racetracks are turned off. There would then be no possibility that turn-off transients not well understood could eject a trapped $\bar{p}$, for example.

This section considers whether any $\bar{p}$ could acquire enough cyclotron energy to be mirror-trapped at the time that $\overline{\mathrm{H}}$ are released for detection. The previous section concluded that to be mirror-trapped a $\bar{p}$ would need to acquire at least 137 eV of cyclotron energy (more than 10^6 K in temperature units) for a $\bar{p}$ located on-axis between electrodes UTR3 and UTR4 (Fig. 6). For most $\bar{p}$ locations, and for $E_T > 0$, even more than this high cyclotron energy would be required.

Evaluating the cyclotron energy that a $\bar{p}$ would have to have at the time at which $\overline{\mathrm{H}}$ atoms are released from the trap requires a brief consideration of some aspects of the capture and cooling of $\bar{p}$. These familiar processes have been described elsewhere [21]. Possible thermal and nonthermal excitations of $\bar{p}$ cyclotron motion are considered, along with the ionization of $\overline{\mathrm{H}}$ atoms.

A. Cooled and uncooled $\bar{p}$

The $\bar{p}$ for these measurements are initially captured by ATRAP in a 5-keV potential well, whereupon they can have translational energies along 3.7 T magnetic field lines up to the well depth. Insofar as some trapped $\bar{p}$ could have cyclotron energies that are similarly large they would be candidates for mirror trapping.

Most of the initially captured $\bar{p}$ collide with cold trapped electrons [21]. This electron cooling thermalizes both the $\bar{p}$ cyclotron energy and the $\bar{p}$ translational energy along magnetic field lines. As discussed in the following section, the thermalized cyclotron energy is much too small for mirror trapping.

Any $\bar{p}$ that is radially outside the cold electron plasma does not collide with the electrons and is thus not electron-cooled. Uncooled $\bar{p}$ with large cyclotron energies are actually ejected from the trap volume not long after the $\bar{p}$ are initially captured in the ATRAP Penning trap (long before the Ioffe racetrack current is turned off to let trapped $\overline{\mathrm{H}}$ atoms escape). The loss takes place when the magnetic field $B_i = 3.7$ T in which the $\bar{p}$ are initially captured is adiabatically reduced to $B_f = 1$ T. The ratio of the cyclotron energy and the magnetic field is an adiabatic invariant, as discussed earlier. As a result the $\bar{p}$ cyclotron energy reduces from E_{ci} to $E_{cf} = E_{ci}(B_f/B_i)$. The lost cyclotron energy increases the translational energy along the magnetic field lines by $\Delta E = E_{cf}(B_i/B_f - 1) = 2.7E_{cf}$. Thus $E_{cf} = 137$ eV is only possible for a translational energy greater than 370 eV.

After the magnetic field reduction, the well depth for the Penning trap is only 10 eV, ensuring that $\bar{p}$ with enough cyclotron energy for later mirror trapping are ejected from the trap. A $\bar{p}$ with more than about 4 eV of cyclotron energy would have acquired enough energy to escape the 10-eV well.

When the Ioffe trap is turned on the magnetic field increases to 2.1 T. The cyclotron energy increases in proportion but would still be very much less than what is needed for mirror trapping.

B. Thermal $\bar{p}$

After catching, cooling, and transferring $\bar{p}$ to a nested Penning trap, the $\bar{p}$ temperature before $\overline{\mathrm{H}}$ formation has been directly measured to be 31 K (as part of a study of subsequent adiabatic cooling [22]). For a $\bar{p}$ density of 10^6 cm^{-3}, the isotropization rate between axial and cyclotron energy is 330 Hz at our magnetic field [23], which is fast enough to ensure that the axial and cyclotron temperatures remain in thermal equilibrium with each other. For a thermal distribution of cyclotron energies centered around $E_c = 31$ K $= 2.7$ meV, the probability of having $E_c > 137$ eV is negligibly small.

C. Driven $\bar{p}$

Forming $\overline{\mathrm{H}}$ requires increasing the amplitude of the motion of the $\bar{p}$ along the magnetic field lines to bring them into contact with the e^+ plasma. To this end, radio-frequency electric fields are applied to drive this $\bar{p}$ motion. To keep the drives near resonance with the $\bar{p}$ oscillation along the magnetic field lines, the drive frequency is either chirped or broadened by noise. The $\bar{p}$ cyclotron energy is not directly excited, since applied oscillating electric fields are far off resonance and are cylindrically symmetric. Instead, the $\bar{p}$ gain translational energy along magnetic field lines, and collisions equilibrate the translational and cyclotron motions, leaving them both in a thermal distribution at the same temperature.

For every set of drive parameters used, the axial $\bar{p}$ temperature has been measured following their excitation. In the most extreme case, when the strongest noise-broadened drive was applied for 10 min, the $\bar{p}$ axial (and hence cyclotron) energy was found to be 1 eV. For a thermal distribution at this energy, for example, only a single $\bar{p}$ out of 10^6 has a cyclotron energy larger than 15 eV. Since all $\bar{p}$ with $E_c <$ 137 eV are ejected by the clearing electric field, the probability that a single $\bar{p}$ could remain mirror-trapped is negligible.

Upper bounds on the translational energy can also be set by observing $\bar{p}$ loss rates. Approximately 500 out of 10^6 $\bar{p}$ in a 3-eV thermal distribution, for example, would have enough translational energy to escape the 27-eV-deep nested well. Since such loss is not observed, the $\bar{p}$ energy must always be less than 3 eV (consistent with our direct measurements). Even more stringent bounds may be placed by observing the number of $\bar{p}$ escaping over the 5-eV central nested well barrier, with the result that in all cases the probability of creating a mirror-trapped $\bar{p}$ during the drive is negligible.

As the $\bar{p}$ mix with e^+ to form $\overline{\mathrm{H}}$, they are likely to lose cyclotron energy since the two species equilibrate at a rate faster than the recombination rate. The e^+ cooling of $\bar{p}$ has long been demonstrated [24], with a collisional cooling rate of approximately 100 s^{-1} for an e^+ plasma with a density of 5×10^7 cm^{-3} in a 2.2-T magnetic field [25]. At the 31 K e^+ temperature, the three-body recombination rate [13] is nearly 2 orders of magnitude smaller than the collisional cooling rate. This affords sufficient time for any $\bar{p}$ with large amounts of cyclotron energy to lose it in collisions with the e^+.

D. Ionized $\overline{\mathrm{H}}$

Most of the $\overline{\mathrm{H}}$ atoms produced are in highly excited states that can be ionized with a laboratory electric field. A $\bar{p}$ from an ionized $\overline{\mathrm{H}}$ atom could have most of the kinetic energy of the $\overline{\mathrm{H}}$, along with any energy acquired by acceleration of the $\bar{p}$ after ionization.

The energy distribution of the $\bar{p}$ produced by the ionization of an $\overline{\mathrm{H}}$ atom is predominantly the energy distribution of the $\bar{p}$ from the $\overline{\mathrm{H}}$ formed. The reasons that $\bar{p}$ have much less than 137 eV of cyclotron energy have already been discussed.

A $\bar{p}$ from $\overline{\mathrm{H}}$ ionization oscillates along a magnetic field line with an energy that arises from the electrical potential where the ionization takes place, possibly increased slightly by the small kinetic energy from the $\overline{\mathrm{H}}$ motion just considered. At most, this conveys 40 eV of energy (if the ionization takes place just inside the electrode wall and if the $\bar{p}$ avoids striking an electrode surface). Collisions with e^+ or other $\bar{p}$ are much too rare to convert this oscillation energy into cyclotron energy and to boost the cyclotron energy above 137 eV.

No plausible way that $\overline{\mathrm{H}}$ ionization can produce the minimum 137 eV of $\bar{p}$ cyclotron energy that is required for mirror trapping has thus been identified.

V. CONCLUSION

In conclusion, the signals that establish that an average of five $\overline{\mathrm{H}}$ atoms per trial have been confined in a quadrupole Ioffe trap for 15 to 1000 s seem to be properly attributed to $\overline{\mathrm{H}}$ atoms rather than to mirror-trapped $\bar{p}$ that are released at the same time. The mirror-trap field is not turned off when $\overline{\mathrm{H}}$ atoms are released to make it less likely that mirror-trapped $\bar{p}$, if some did exist, would be released with the trapped $\overline{\mathrm{H}}$. In addition, this study shows that a minimum of 137 eV of cyclotron energy (more than 10^6 K in temperature units) must be given to a $\bar{p}$ for it to be mirror-trapped in ATRAP's Ioffe trap. Much more cyclotron energy is required at most $\bar{p}$ locations in the Penning-Ioffe trap and for $\bar{p}$ with translational energy. No plausible source of such high cyclotron energies has been identified.

ACKNOWLEDGMENTS

We are grateful to CERN for delivering the 5-MeV $\bar{p}$ from its unique Antiproton Decelerator. This work was supported by the NSF and the AFOSR of the United States; the NSERC, the CRC, the CFI, and the OIT of Canada; and the BMBF and the DFG of Germany.

[1] G. Gabrielse, R. Kalra, W. S. Kolthammer, R. McConnell, P. Richerme, D. Grzonka, W. Oelert, T. Sefzick, M. Zielinski, D. W. Fitzakerley, M. C. George, E. A. Hessels, C. H. Storry, M. Weel, A. Müllers, and J. Walz, Phys. Rev. Lett. **108**, 113002 (2012).

[2] G. B. Andresen *et al.* (ALPHA Collaboration), Nat. Phys. **7**, 558 (2011).

[3] G. Gabrielse, in *Fundamental Symmetries*, edited by P. Bloch, P. Pavlopoulos, and R. Klapisch (Plenum, New York, 1987), pp. 59–75.

[4] C. Zimmermann and T. W. Hänsch, Hyperfine Interact. **76**, 47 (1993).
[5] G. Gabrielse, Hyperfine Interact. **44**, 349 (1988).
[6] D. E. Pritchard, Phys. Rev. Lett. **51**, 1336 (1983).
[7] R. C. Davidson, *Physics of Non-neutral Plasmas* (Imperial College Press, London, 2001).
[8] J. C. Wesley and A. Rich, Phys. Rev. A **4**, 1341 (1971).
[9] H. Boehmer, M. Adams, and N. Rynn, Phys. Plasmas **2**, 4369 (1995).
[10] J. A. P. Mills, Appl. Phys. **22**, 273 (1980).
[11] C. Amole *et al*. (ALPHA Collaboration), New J. Phys. **14**, 015010 (2012).
[12] G. Gabrielse, L. Haarsma, and S. L. Rolston, Int. J. Mass Spectrom. Ion Processes **88**, 319 (1989); **93**, 121 (1989).
[13] G. Gabrielse, S. L. Rolston, L. Haarsma, and W. Kells, Phys. Lett. A **129**, 38 (1988).
[14] M. Glinsky and T. O'Neil, Phys. Fluids B **3**, 1279 (1991).
[15] G. Gabrielse, Adv. At. Mol. Opt. Phys. **50**, 155 (2005).
[16] T. Pohl, H. R. Sadeghpour, Y. Nagata, and Y. Yamazaki, Phys. Rev. Lett. **97**, 213001 (2006).
[17] F. Robicheaux, Phys. Rev. A **73**, 033401 (2006).
[18] T. M. Squires, P. Yesley, and G. Gabrielse, Phys. Rev. Lett. **86**, 5266 (2001).
[19] T. Northrop, *The Adiabatic Motion of Charged Particles* (Wiley, New York, 1963).
[20] R. G. Littlejohn, Phys. Fluids **24**, 1730 (1981).
[21] G. Gabrielse, Adv. At. Mol. Opt. Phys. **45**, 1 (2001).
[22] G. Gabrielse, W. S. Kolthammer, R. McConnell, P. Richerme, R. Kalra, E. Novitski, D. Grzonka, W. Oelert, T. Sefzick, M. Zielinski, D. Fitzakerley, M. C. George, E. A. Hessels, C. H. Storry, M. Weel, A. Müllers, and J. Walz (ATRAP Collaboration), Phys. Rev. Lett. **106**, 073002 (2011).
[23] M. E. Glinsky, T. M. O'Neil, M. N. Rosenbluth, K. Tsurula, and S. Ichimaru, Phys. Fluids B **4**, 1156 (1992).
[24] G. Gabrielse *et al*., Phys. Lett. B **507**, 1 (2001).
[25] J. L. Hurt, P. T. Carpenter, C. L. Taylor, and F. Robicheaux, J. Phys. B **41**, 165206 (2008).

References

[1] J. Ellis, N. E. Mavaromatos, and D. V. Nanopoulos, Phys. Lett. B **293**, 142 (1992).

[2] V. A. Kostelecký and R. Potting, Nucl. Phys. **B359**, 545 (1991).

[3] D. Colladay and V. A. Kostelecký, Phys. Rev. D **55**, 6760 (1997).

[4] R. Bluhm, V. A. Kostelecký, and N. Russell, Phys. Rev. Lett. **82**, 2254 (1999).

[5] G. Gabrielse, D. Phillips, W. Quint, H. Kalinowsky, G. Rouleau, and W. Jhe, Phys. Rev. Lett. **74**, 3544 (1995).

[6] R. S. Van Dyck, Jr., P. B. Schwinberg, and H. G. Dehmelt, Phys. Rev. Lett. **59**, 26 (1987).

[7] R. Carosi *et al.*, Phys. Lett. B **237**, 303 (1990).

[8] C. Zimmermann and T. Hänsch, Hyperfine Interact. **76**, 47 (1993).

[9] C. Parthey *et al.*, Phys. Rev. Lett. **107**, 203001 (2011).

[10] F. Schmidt-Kaler, D. Leibfried, S. Seel, C. Zimmermann, W. König, M. Weitz, and T. W. Hänsch, Phys. Rev. A **51**, 2789 (1995).

[11] C. L. Cesar, D. G. Fried, T. C. Killian, A. D. Polcyn, J. C. Sandberg, I. A. Yu, T. J. Greytak, D. Kleppner, and J. M. Doyle, Phys. Rev. Lett. **77**, 255 (1996).

[12] R. J. Hughes, Hyperfine Interact. **76**, 3 (1993).

[13] G. Gabrielse, Hyperfine Interact. **44**, 349 (1988).

[14] P. D. Lett, R. N. Watts, C. I. Westbrook, W. D. Phillips, P. L. Gould, and H. J. Metcalf, Phys. Rev. Lett. **61**, 169 (1988).

[15] J. Walz and T. Hänsch, Gen. Rel. Grav. **36**, 561 (2004).

[16] G. Gabrielse, A. Khabbaz, D. S. Hall, C. Heimann, H. Kalinowsky, and W. Jhe, Phys. Rev. Lett. **82**, 3198 (1999).

[17] R. J. Hughes and M. H. Holzscheiter, Phys. Rev. Lett. **66**, 854 (1991).

[18] G. Gabrielse, X. Fei, K. Helmerson, S. L. Rolston, R. L. Tjoelker, T. A. Trainor, H. Kalinowsky, J. Haas, and W. Kells, Phys. Rev. Lett. **57**, 2504 (1986).

[19] G. Gabrielse, X. Fei, L. A. Orozco, R. L. Tjoelker, J. Haas, H. Kalinowsky, T. A. Trainor, and W. Kells, Phys. Rev. Lett. **65**, 1317 (1990).

[20] G. Gabrielse *et al.*, Phys. Lett. B **548**, 140 (2002).

[21] G. Gabrielse, in *Fundamental Symmetries*, edited by P. Bloch, P. Pavlopoulos, and R. Klapisch (Plenum, New York, 1987), pp. 59–75.

[22] N. Guise, J. DiSciacca, and G. Gabrielse, Phys. Rev. Lett. **104**, 143001 (2010).

[23] J. DiSciacca and G. Gabrielse, Phys. Rev. Lett. **108**, 153001 (2012).

[24] J. DiSciacca and et al., Phys. Rev. Lett. **110**, 130801 (2013).

[25] J. DiSciacca, M. Marshall, K. Marable, and G. Gabrielse, Phys. Rev. Lett. **110**, 140406 (2013).

[26] G. Gabrielse *et al.*, Phys. Rev. Lett. **108**, 113002 (2012).

[27] P. Richerme *et al.*, **87**, 023422 (2013).

[28] M. Niering *et al.*, Phys. Rev. Lett. **84**, 5496 (2000).

[29] D. Hanneke, S. Fogwell, and G. Gabrielse, Phys. Rev. Lett. **100**, 120801 (2008).